separations

MDPI

Article

Untargeted UHPLC–HRMS/MS Profiling of Secondary Metabolites in Roots and Aerial Parts of *Plagiorhegma dubium*

Roman S. Popov [1,*], Natalia V. Ivanchina [1], Elena V. Novozhilova [1], Roman V. Dudkin [1,2] and Pavel S. Dmitrenok [1,*]

[1] G.B. Elyakov Pacific Institute of Bioorganic Chemistry, Far Eastern Branch of Russian Academy of Sciences, 159 Prospect 100-letiya Vladivostoku, Vladivostok 690022, Russia; ivanchina@piboc.dvo.ru (N.V.I.)
[2] Botanical Garden-Institute, Far Eastern Branch of Russian Academy of Sciences, 142 Makovsky St., Vladivostok 690022, Russia
* Correspondence: popov_rs@piboc.dvo.ru (R.S.P.); paveldmt@piboc.dvo.ru (P.S.D.); Tel.: +7-423-231-1132 (P.S.D.)

Abstract

Plagiorhegma dubium is an underexplored member of Berberidaceae whose secondary metabolite composition and distribution between plant organs remain poorly characterized. Here, untargeted UHPLC-ESI-QTOF-HRMS/MS combined with feature-based molecular networking was applied to profile and obtain putative structural annotations of major metabolite families in the roots and aerial parts of *P. dubium*. The analysis revealed marked differences between root and aerial-part metabolite profiles and enabled annotation of 14 alkaloid-related features, 61 putative triterpenoid saponins, and 17 flavonoid, hydroxycinnamate, and related metabolites. Among the annotated alkaloids, magnoflorine strongly dominated the root profile, whereas jatrorrhizine/columbamine-type protoberberines were enriched in the aerial-part profile. LC–MS/MS data revealed an extensive family of structurally diverse triterpene saponins, a metabolite class not previously reported from *P. dubium*. The saponins comprised multiple aglycones, glycan, and non-carbohydrate substituent combinations, with $C_{30}H_{46}O_6$-type aglycones enriched in roots and the more highly oxygenated $C_{30}H_{46}O_7$ family predominant in aerial parts. Flavonoid glycosides and hydroxycinnamate derivatives were strongly enriched in the aerial parts. These findings substantially expand the known phytochemical diversity of *P. dubium* and identify it as a rich source of structurally unresolved metabolites requiring isolation and definitive structure elucidation.

Keywords: *Plagiorhegma dubium*; Berberidaceae; UHPLC-HRMS/MS; feature-based molecular networking; benzylisoquinoline alkaloids; triterpene glycosides (saponins); flavonoid glycosides; hydroxycinnamate derivatives

Check for updates

Academic Editor: Liangliang Liu

Received: 12 September 2026
Revised: 23 October 2026
Accepted: 30 October 2026
Published: 2 November 2026

Copyright: © 2026 by the authors. Licensee MDPI, Basel, Switzerland. This article is an open access article distributed under the terms and conditions of the Creative Commons Attribution (CC BY) license.

1. Introduction

Plants produce a remarkable diversity of secondary metabolites whose occurrence often shows taxonomic, organ, and developmental specificity. These compounds encompass several major structural classes, including alkaloids, phenolic compounds, terpenes, steroids, and their glycosides. Secondary metabolites contribute to numerous ecological and physiological processes, including defense against herbivores and pathogens, adaptation to abiotic stress, signaling, and interactions with other organisms [1]. Many of these compounds also exhibit pronounced biological activities and constitute an important source of lead compounds and structural scaffolds for drug discovery and development [2,3]. Their qualitative and quantitative profiles may differ substantially among species and between

organs or developmental stages within the same plant, reflecting tissue-specific biosynthesis, transport, accumulation, and regulation of secondary metabolism [1,4].

The family Berberidaceae currently comprises 13 genera [5] and exhibits considerable phytochemical diversity across several major classes of secondary metabolites. Species of *Berberis* are well known for the accumulation of benzylisoquinoline alkaloids, including berberine, palmatine, jatrorrhizine, aporphines such as magnoflorine, and bisbenzylisoquinoline alkaloids such as berbamine and oxyacanthine [6,7]. Phytochemical investigations of *Epimedium* species have led to the isolation and identification of numerous flavonoids, particularly prenylated flavonoids and their glycosides, including icariin, icaritin, and many structurally related compounds [8]. Species of the *Podophyllum* group are particularly rich in aryltetralin lignans, including podophyllotoxin, which serves as a precursor for the semisynthesis of the clinically used anticancer agents etoposide and teniposide [9,10]. Other representatives of Berberidaceae, such as *Caulophyllum*, accumulate abundant triterpenes and structurally diverse triterpene saponins [11]. Thus, the family combines several major biosynthetic directions of plant secondary metabolism and represents a valuable group for comparative phytochemical and chemotaxonomic studies. Many of these metabolite classes exhibit biologically relevant activities. Individual isoquinoline alkaloids occurring in *Berberis*, including berberine, palmatine, jatrorrhizine, magnoflorine, and berbamine, have been associated with antimicrobial, anti-inflammatory, antioxidant, and antiproliferative activities [7,12]. Polyphenolic constituents, including flavonoids and phenolic acids, also contribute to the biological activity of Berberidaceae extracts. In *Berberis*, these compounds have been associated with antioxidant, antimicrobial, and enzyme-inhibitory effects, whereas prenylated flavonoids from *Epimedium* have been investigated for a range of pharmacological activities [8,12]. Triterpene saponins isolated from *Caulophyllum* species have been reported to exhibit anti-inflammatory and other pharmacological activities [13].

Plagiorhegma dubium Maxim. (syn. *Jeffersonia dubia* (Maxim.) Benth. & Hook.f. ex Baker & Moore) is a perennial rhizomatous herb of the family Berberidaceae, distributed in temperate East Asia, including the Russian Far East, northeastern China, and the Korean Peninsula. It is a spring-flowering forest plant adapted to shaded habitats and has attracted attention as both an ornamental and a potentially medicinal species. The species has been used in traditional medicine for the treatment of several conditions, including diabetes, gastrointestinal disorders, dysentery and inflammatory eye disorders [14,15]. Despite extensive phytochemical and pharmacological studies of several other representatives of Berberidaceae, the chemical composition of *P. dubium* remains poorly investigated. Early phytochemical studies of *P. dubium* were largely focused on alkaloids. Arens et al. isolated the protoberberine alkaloid jatrorrhizine together with two lignan glycosides from cultured cells [16]. Jeong and Sivanesan confirmed the presence of berberine by HPLC and demonstrated differences in its content among in vitro-grown shoots, callus cultures, and leaves of field-grown plants [17]. More recently, Sun et al. analyzed a methanolic extract of the underground parts of *P. dubium* by UHPLC-ESI MS and reported 41 compounds, 38 of which were putatively assigned as alkaloids, with magnoflorine, berberrubine, and betaine reported as the major constituents [14]. Thus, previous studies focused either on cultured material, targeted analysis of individual alkaloids, or the underground organs of the plant, whereas the broader secondary metabolite composition and organ-dependent distribution of metabolites in *P. dubium* remain insufficiently characterized.

The limited phytochemical information available for *P. dubium* is particularly notable in comparison with other representatives of Berberidaceae, for which modern LC-MS approaches have revealed highly complex metabolite profiles. Recent UHPLC-MS studies of Berberis species have revealed chemically diverse profiles comprising isoquinoline alkaloids, phenolic acids, flavonoids, lignans, and other metabolites [12,18]. LC-MS profiling of

Caulophyllum has enabled characterization of structurally diverse triterpene saponins [19]. These studies illustrate that information based on a limited number of previously isolated compounds may substantially underestimate the phytochemical diversity of a plant.

Traditional phytochemical studies rely on isolation of individual compounds followed by structure elucidation using NMR, MS, and complementary spectroscopic methods. Although essential for unambiguous characterization of novel structures, these approaches are labor-intensive, require substantial amounts of material, and may overlook minor constituents. LC-HRMS/MS has therefore become a major tool for comprehensive phytochemical profiling [20,21]. Accurate mass measurements, isotopic patterns, and MS/MS fragmentation support elemental composition assignment and structural annotation, while comparison with authentic standards, spectral libraries, and literature data facilitates dereplication of known compounds. Feature-based molecular networking further facilitates organization of complex LC-MS/MS datasets into groups of spectrally related features while retaining chromatographic and quantitative information, thereby supporting recognition and annotation of structurally related metabolite families [22]. This approach is particularly suitable for untargeted analysis of poorly characterized plant species and for comparison of metabolite profiles. However, positional and stereochemical isomers and glycosidic linkage positions often cannot be resolved by MS/MS alone; therefore, annotations made without authentic standards remain putative [23].

In the present study, untargeted UHPLC–ESI–QTOF–HRMS/MS combined with feature-based molecular networking was applied to compare the metabolite profiles of the roots and aerial parts of *P. dubium*. This study aimed to comprehensively profile secondary metabolites in the roots and aerial parts of *P. dubium*, organize structurally related features using molecular networking, obtain putative structural annotations for the major metabolite families, and characterize differences in their relative distribution between the two organs. The resulting data provide a basis for targeted isolation and definitive structure elucidation of structurally distinctive metabolites and for future comparative phytochemical studies within Berberidaceae.

2. Materials and Methods

2.1. Chemicals and Reagents

MS-grade acetonitrile and methanol were purchased from EvaScience (Saint Petersburg, Russia). Dichloromethane was purchased from Merck (Darmstadt, Germany). Ultrapure water was produced using an aquaMAX Ultra 370 Series water purification system (YoungIn Chromass, Anyang, Republic of Korea). MS-grade formic acid was purchased from neoFroxx (Einhausen, Germany).

2.2. Plant Materials

Ten mature individuals of *Plagiorhegma dubium* Maxim. (syns. *Jeffersonia dubia* (Maxim.) Benth & Hook.f. ex Baker & Moore and *Jeffersonia manchuriensis* Hance) were collected in September 2025 from a forest site in the Lazurnaya River valley near Vladivostok, Primorsky Krai, Russia. The plant material was identified by Elena V. Novozhilova and Roman V. Dudkin. A voucher specimen (ID 142627/1983) was deposited in the Herbarium of the Botanical Garden-Institute, Vladivostok, Russia.

2.3. Sample Preparation and Extraction

The collected plants were separated into roots and aerial parts (leaves and petioles), and the corresponding organs from the ten individuals were pooled separately to obtain one composite root sample and one composite aerial-part sample. The plant material was

cleaned, air-dried in a cool, well-ventilated place, and subsequently dried in an oven at 45 °C for 30 h. The dried root and aerial-part materials were ground separately to a powder.

Previous phytochemical studies of *P. dubium* primarily employed methanol-based extraction. Arens et al. [16] investigated a methanolic extract of cultured plant cells, whereas Sun et al. [14] compared water, methanol, and ethanol extracts of underground plant parts and selected methanol for subsequent LC-MS analysis based on extraction yield and total alkaloid content. In contrast, the present study aimed to obtain broad coverage of secondary metabolites with different polarities. Therefore, preliminary extraction experiments were performed using ethanol, methanol, aqueous methanol mixtures, chloroform, and dichloromethane. Among the tested approaches, sequential extraction with dichloromethane followed by methanol yielded the broadest detectable LC-MS profile, with the largest number of chromatographic peaks and generally higher signal intensities in both positive- and negative-ion modes. Accordingly, the dichloromethane and methanol extracts were combined for subsequent untargeted LC-MS/MS profiling.

One extract was prepared from each pooled plant sample (roots and aerial parts). A 1.0 g portion of each powdered sample was extracted by maceration with 8 mL of dichloromethane at room temperature for 12 h, with occasional manual shaking. After centrifugation for 5 min at 1000 rpm (~200× g), the supernatant was collected, and the remaining plant residue was extracted with 7 mL of methanol at room temperature for 6 h. After centrifugation under the same conditions, the methanolic extract was collected and the residue was subjected to a second extraction with 7 mL of methanol for 6 h. The three extracts obtained from each sample were combined, filtered, and evaporated to dryness under a stream of nitrogen. The dried residues were weighed, yielding 207.0 mg from the root sample and 148.9 mg from the aerial-part sample. Each dry extract was reconstituted in 10 mL of acetonitrile/methanol/water (4:4:2, $v/v/v$). Prior to UHPLC–MS analysis, an aliquot of each reconstituted extract was filtered through a 0.2 µm PVDF microcentrifugal filter (cat. no. F2517-5; Thermo Fisher Scientific, Waltham, MA, USA).

2.4. UHPLC–HRMS/MS Analysis

UHPLC–HRMS/MS analysis was performed using a Bruker Elute UHPLC system (Bruker Daltonics, Bremen, Germany) comprising an Elute Pump HPG 1300, an Elute Autosampler UHPLC, and an Elute Column Oven, coupled to an Impact II QTOF mass spectrometer (Bruker Daltonics, Bremen, Germany) equipped with an electrospray ionization (ESI) source. Chromatographic separation was performed using an Acquity UPLC HSS T3 column (150 × 2.1 mm, 1.8 µm, 100 Å; Waters Corporation, Milford, MA, USA) equipped with an Acquity UPLC HSS T3 VanGuard pre-column (5 × 2.1 mm, 1.8 µm, 100 Å; Waters Corporation, Milford, MA, USA). The mobile phases were 0.1% (v/v) formic acid in water (eluent A) and 0.1% (v/v) formic acid in acetonitrile (eluent B). The gradient was programmed as follows: 5–20% B (0–2 min), 20–80% B (2–22 min), 80–100% B (22–24 min), isocratic at 100% B (24–27 min), then reduced to 5% B (27.0–27.2 min). The column was re-equilibrated for 3.8 min before the next injection. The flow rate was 0.4 mL/min, the column temperature was 45 °C and the injection volume was 4 µL in the partial loop injection mode.

Mass spectrometric detection was performed using ESI in separate positive- and negative-ion runs. Optimized ionization parameters were set as follows: a capillary voltage of 4.0 kV in negative-ion mode and 4.5 kV in positive-ion mode; nebulizer gas (N_2), 2.0 bar; dry gas (N_2), 8 L/min; dry gas temperature, 210 °C. Mass spectra were acquired in the m/z range of 80–1700 at 2 Hz. Collision-induced dissociation (CID) product-ion spectra were recorded in the autoMS/MS mode at 3 Hz, with the two most intense precursor ions selected from each survey scan and an isolation width of 4 Th. The nominal collision energy was varied as a function of precursor m/z: 15 eV at m/z 100, 35 eV at m/z 200, 50 eV at

m/z 400, 95 eV at m/z 800, and 120 eV at m/z 1000. Collision energy Stepping option was applied, acquiring 50% of each MS/MS scan at 60% of the set collision energy, in order to obtain the most informative fragmentation spectra. Active exclusion was enabled after two MS/MS spectra had been acquired for a given precursor ion. The instrument was calibrated using the ESI-L Low Concentration Tuning Mix (Agilent Technologies, Santa Clara, CA, USA). The mass spectrometer was operated using otofControl (ver. 4.1, Bruker Daltonics, Bremen, Germany). The DataAnalysis software (ver. 4.3, Bruker Daltonics, Bremen, Germany) was used for analyzing the MS data and for generation of molecular formulas using the SmartFormula module with a 10-ppm error window. Each extract was analyzed in triplicate in both positive- and negative-ion modes. Peak areas obtained from the three technical replicate injections were averaged, and the resulting mean values were used for comparisons between the root and aerial-part extracts. Blank samples were analyzed to evaluate background signals, contaminants, and sample carryover. Features corresponding to background contaminants, including phthalate-related signals, were manually identified by comparison with blank chromatograms and excluded from the final feature lists. No detectable carryover was observed.

The LC-MS raw data files were converted to the open mzML format using ProteoWizard MSConvert (ver. 3.0.23009, ProteoWizard, Palo Alto, CA, USA) [24]. The mzML files were processed separately for positive- and negative-ion datasets using MZmine 2.53 [25] for feature detection, chromatographic alignment, and MS/MS data export. Detailed MZmine processing parameters are provided in Supplementary Table S4. For each ionization mode, an aligned feature quantification table (.csv) and an MS/MS spectral summary file (.mgf) were exported for subsequent analysis. Separate molecular networks for the positive- and negative-ion datasets were generated using the Feature-Based Molecular Networking (FBMN) workflow [22] (version release_28.2) on the GNPS platform [26]. The precursor-ion and fragment-ion mass tolerances were set to 0.01 and 0.02 Da, respectively. Network edges were retained when the cosine similarity score exceeded 0.7 and at least five fragment ions were matched. An edge was retained only when each connected node occurred among the ten most similar spectra of the other node. The maximum molecular family size was set to 100 nodes; for larger families, the lowest-scoring edges were sequentially removed until the number of nodes was below this threshold. The resulting molecular networks were visualized using Cytoscape (version 3.9.1) [27]. The GNPS jobs for the positive- and negative-ion datasets can be accessed at https://gnps.ucsd.edu/ProteoSAFe/status.jsp?task=323d8eb2a14b4b04907b0eee55ddad24 (accessed on 1 September 2026) and https://gnps.ucsd.edu/ProteoSAFe/status.jsp?task=041f9892f911410087ae0efe713a6680 (accessed on 1 September 2026), respectively.

In this study, an LC-MS feature refers to a chromatographic signal characterized by a specific retention time and m/z ratio. Features for which sufficient spectral evidence was available were assigned putative metabolite annotations. Metabolite annotation confidence was assessed according to the Metabolomics Standards Initiative (MSI) guidelines. Putative annotations of specific compounds supported by accurate-mass measurements, characteristic MS/MS fragmentation patterns, and comparison with published reference spectra in MS/MS databases and related articles were classified as MSI Level 2. Features for which the available evidence supported only a compound class, structural family, or a group of possible isomers were classified as MSI Level 3.

3. Results

LC-MS analysis revealed complex and markedly different profiles for the root and aerial-part extracts of *P. dubium* (Figure S1). In negative-ion mode, the base-peak chromatograms of both roots and aerial parts contained numerous partially overlapping peaks, reflecting

the high complexity of the negative-ion LC-MS profiles. Despite their similarly complex appearance, the two profiles differed markedly. In positive-ion mode, the difference was even more apparent: the root profile was dominated by a single major peak accompanied by numerous substantially less intense signals, whereas the aerial-part profile contained several prominent peaks of comparable intensity.

To examine the structural relationships among the detected components, feature-based molecular networks were generated independently for the positive- and negative-ion LC-MS/MS datasets (Figures S2 and S3, respectively). The positive-ion network comprised six molecular families with at least four nodes; the two largest families contained 55 and 14 features, respectively. The negative-ion dataset showed a more extensive clustering pattern, with 13 molecular families containing at least four nodes; the two largest molecular families comprised 88 and 28 features, respectively. In addition to these families, both networks contained numerous smaller clusters, pairs, and singleton features, indicating substantial spectral heterogeneity within both datasets. Several positive-ion molecular families contained features putatively annotated as isoquinoline alkaloids, whereas the major annotated families in the negative-ion network were associated with putative triterpene saponins, flavonoid glycosides, and hydroxycinnamate-related metabolites. The relative peak-area contributions of the root and aerial-part extracts varied markedly both within and among molecular families, indicating substantial differences in the distribution of structurally related features between the two plant parts. Features belonging to the major metabolite families were subsequently subjected to structural annotation based on accurate-mass measurements, MS/MS fragmentation patterns, spectral similarity, and comparison with available reference data, as described below. This workflow resulted in the putative annotation of 92 LC-MS features, including 14 alkaloid-related, 61 triterpene saponin-related, and 17 flavonoid-, hydroxycinnamate-, and related features. All annotations were based on accurate-mass measurements, MS/MS fragmentation patterns, and comparison with available reference data.

3.1. Alkaloids

In total, 14 alkaloid-related LC-MS features were putatively annotated in the positive-ion data. Eleven of these were distributed among three alkaloid-associated molecular families (P5, P10, and P11), whereas three occurred as singleton nodes (Figures 1, S4 and S5, Tables 1 and S1). The annotations encompassed several structural classes of benzylisoquinoline-derived alkaloids, including monomeric and putative dimeric protoberberines, aporphines, and benzyltetrahydroisoquinoline alkaloids. Feature **A5** (m/z 342.17, Rt = 3.61 min), the dominant alkaloid-related feature in the root extract accounting for >82% of the summed LC-MS signal of the annotated alkaloid-related features in the root extract, was assigned to molecular cluster P11 together with two related nodes interpreted as a dimeric ion and an in-source fragment. Its MS/MS spectrum closely matched published MS/MS data for magnoflorine and exhibited the characteristic fragmentation behavior of a quaternary aporphine alkaloid. The dominant product ion at m/z 297.11 resulted from a neutral loss of 45.06 Da, consistent with C_2H_7N. This dissociation pathway has been reported for magnoflorine and related *N*,*N*-dimethyl-substituted aporphine alkaloids [28,29]. Subsequent elimination of CH_3OH produced the abundant product ion at m/z 265.09, followed by loss of CO to yield the ion at m/z 237.09. This sequential CH_3OH/CO elimination is consistent with the vicinal hydroxy/methoxy substitution pattern of the aporphine aromatic system. The product ion at m/z 282.09 was consistent with secondary loss of a methyl radical from the m/z 297.11, whereas additional ions at m/z 247.07, 222.07, and 165.07 were attributed to further dissociation of the aporphine framework. Taken together, the accurate precursor

mass, agreement with previously published fragmentation data, and characteristic MS/MS dissociation pathways supported the putative annotation of **A5** as magnoflorine.

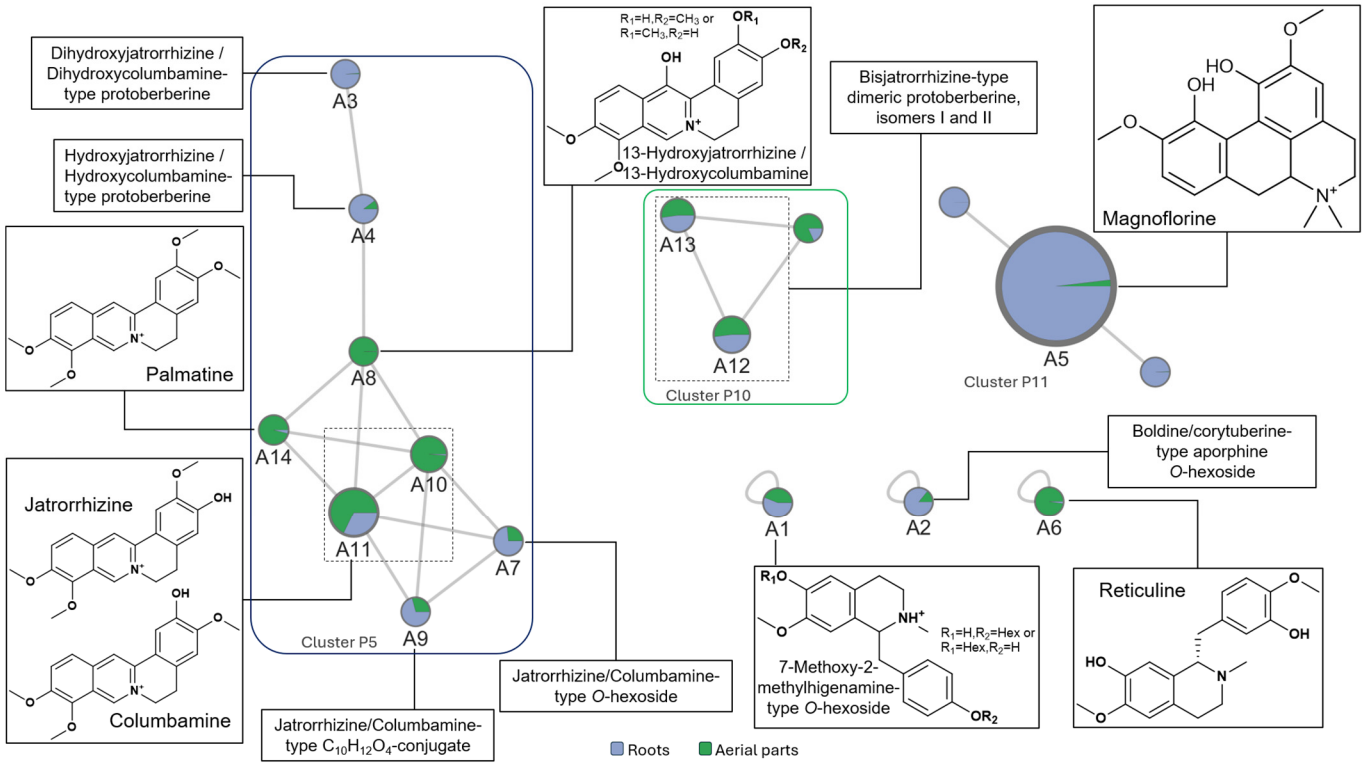


Figure 1. Feature-based molecular network of alkaloid-related features detected in the roots and aerial parts of *P. dubium* by positive-ion LC-ESI-MS/MS. Nodes represent individual features, whereas edges connect features exhibiting similar MS/MS fragmentation patterns. Pie-chart sectors show the relative distribution of the LC-MS signal between root (blue) and aerial-part (green) extracts, and node size is proportional to the summed signal of the corresponding feature. Annotated features are labeled according to the IDs given in Table 1; additional nodes represent unannotated or ion-related features. Structures are shown for representative or putatively annotated metabolites.

Table 1. Putatively annotated alkaloids detected in the roots and aerial parts of *P. dubium* [a].

ID	Measured *m*/*z*	Rt (min)	Ion Formula	Putative Annotation
A1	462.2139	2.73	$[C_{24}H_{32}NO_8]^+$	7-Methoxy-2-methylhigenamine-type *O*-hexoside
A2	490.2081	3.25	$[C_{25}H_{32}NO_9]^+$	Boldine/corytuberine-type aporphine *O*-hexoside
A3	370.1291	3.33	$[C_{20}H_{20}NO_6]^+$	Dihydroxyjatrorrhizine/dihydroxycolumbamine-type protoberberine
A4	354.1339	3.52	$[C_{20}H_{20}NO_5]^+$	Hydroxyjatrorrhizine/hydroxycolumbamine-type protoberberine
A5	342.1712	3.61	$[C_{20}H_{24}NO_4]^+$	Magnoflorine
A6	330.1692	3.78	$[C_{19}H_{24}NO_4]^+$	Reticuline
A7	500.1923	4.08	$[C_{26}H_{30}NO_9]^+$	Jatrorrhizine/columbamine-type *O*-hexoside
A8	354.1341	4.41	$[C_{20}H_{20}NO_5]^+$	13-Hydroxyjatrorrhizine/13-hydroxycolumbamine
A9	534.2132	5.77	$[C_{30}H_{32}NO_8]^+$	Jatrorrhizine/columbamine-type $C_{10}H_{12}O_4$ conjugate
A10	338.1395	5.96	$[C_{20}H_{20}NO_4]^+$	Jatrorrhizine/columbamine isomer I
A11	338.1395	6.11	$[C_{20}H_{20}NO_4]^+$	Jatrorrhizine/columbamine isomer II
A12	337.1324	6.59	$[C_{40}H_{38}N_2O_8]^{2+}$	Bisjatrorrhizine-type dimeric protoberberine, isomer I
A13	337.1324	7.06	$[C_{40}H_{38}N_2O_8]^{2+}$	Bisjatrorrhizine-type dimeric protoberberine, isomer II
A14	352.1550	7.21	$[C_{21}H_{22}NO_4]^+$	Palmatine

[a] The annotations of features **A5**, **A6**, **A8**, **A10**, **A11**, and **A14** were classified as MSI Level 2, whereas all remaining annotations were classified as MSI Level 3.

Molecular family P5 contained eight putatively annotated alkaloids, several of which showed higher relative LC-MS signals in either the roots or aerial parts. Among the features enriched in the aerial parts were two chromatographically resolved isomers, compounds **A10** and **A11**, detected as molecular cations at m/z 338.14 (Rt = 5.96 and 6.11 min, respectively). Both compounds exhibited nearly identical MS/MS spectra characteristic of methoxylated quaternary protoberberine alkaloids. Fragmentation involved the radical loss of $CH_3^{\bullet}$ to yield the product ion at m/z 323.12, whereas the competing neutral loss of CH_4 generated the ion at m/z 322.11. Further fragmentation produced the ion at m/z 307.08, consistent with combined losses of CH_4 and $CH_3^{\bullet}$, while elimination of CO from the m/z 322.11 ion yielded the product ion at m/z 294.11. The related ions at m/z 308.09 and 307.08 underwent further CO loss to give the paired product ions at m/z 280.09 and 279.09, respectively, and subsequent radical loss of $CH_3^{\bullet}$ from the m/z 280.09 ion generated the product ion at m/z 265.07. The predominance of $CH_3^{\bullet}$, CH_4, and CO eliminations is consistent with the well-established fragmentation behavior of methoxylated quaternary protoberberine alkaloids [30]. Accordingly, compounds **A10** and **A11** were tentatively annotated as jatrorrhizine/columbamine isomers based on their elemental composition, characteristic fragmentation, and chemotaxonomic plausibility. These compounds are positional isomers that differ only in the arrangement of the hydroxy- and methoxy-substituents at C-2 and C-3 of ring A; therefore, their individual assignments could not be established unambiguously from the MS/MS data in the absence of authentic standards.

The closest structural analogues of compounds **A10** and **A11** within molecular cluster P5 were features **A14** and **A8**. Feature **A14** was detected as a molecular cation at m/z 352.16 (Rt = 7.21 min). Its elemental composition differed from that of the jatrorrhizine/columbamine isomers by CH_2, a compositional shift consistent with methylation of the remaining phenolic hydroxyl group and formation of a tetramethoxy-substituted protoberberinium alkaloid. The MS/MS spectrum of **A14** closely resembled those of compounds **A10** and **A11**, but the corresponding product-ion series was shifted in accordance with the additional methyl substituent. Radical loss of $CH_3^{\bullet}$ and neutral loss of CH_4 from the molecular cation generated product ions at m/z 337.13 and 336.12, respectively. Subsequent fragmentation produced ions at m/z 322.11, 320.09, 308.13, 294.11, and 292.09 through sequential losses involving $CH_3^{\bullet}$, CH_4, and CO. This fragmentation pattern closely matched published MS/MS data for palmatine, in which the same product-ion series has been reported, and was consistent with the characteristic dissociation behavior of methoxylated quaternary protoberberine alkaloids [29,31,32]. Accordingly, compound **A14** was putatively annotated as palmatine on the basis of its accurate mass, characteristic MS/MS spectrum, and close spectral relationship to the jatrorrhizine/columbamine isomers within molecular cluster P5.

Compound **A8**, another close analogue of compounds **A10** and **A11** within molecular family P5, was detected as a molecular cation at m/z 354.13 (Rt = 4.41 min). Its elemental composition contained one additional oxygen atom relative to the jatrorrhizine/columbamine isomers, while its shorter retention time was consistent with increased polarity associated with the additional oxygenation. The MS/MS spectrum retained the characteristic fragmentation pattern of a methoxylated quaternary protoberberine alkaloid. Radical loss of $CH_3^{\bullet}$ and neutral loss of CH_4 from the molecular cation generated product ions at m/z 339.11 and 338.10, respectively. Additional product ions were observed at m/z 324.08, 306.08, 296.09, and 278.08. This fragmentation pattern closely matched that reported for 13-hydroxycolumbamine/13-hydroxyjatrorrhizine [32,33]. Accordingly, the elemental composition, chromatographic behavior, characteristic MS/MS fragmentation, and close spectral relationship to compounds **A10** and **A11** supported annotation of **A8** as a hydroxylated

jatrorrhizine/columbamine analogue, with 13-hydroxylated structures representing plausible candidates.

Features **A3, A4**, **A7**, and **A9** were preferentially detected in the root extract. Feature **A4** was observed as a molecular cation at m/z 354.13 (Rt = 3.52 min), corresponding to the elemental composition $[C_{20}H_{20}NO_5]^+$ and thus representing an isomer of **A8**. Despite their identical elemental compositions, the two features differ substantially in retention time and fragmentation patterns. The MS/MS spectrum of **A4** was dominated by the fragment at m/z 339.11, corresponding to radical loss of $CH_3^\bullet$ from the precursor, together with prominent ions at m/z 296.09 and 268.09. The mass difference between the ions at m/z 339.11 and 296.09 was consistent with combined loss of $CH_3^\bullet$ and CO, whereas the difference between the ions at m/z 296.09 and 268.09 was consistent with an additional CO loss. The identical elemental compositions, related fragmentation behavior, and co-clustering of features **A4** and **A8** within molecular cluster P5 supported their assignment as isomeric oxygenated protoberberine alkaloids related to jatrorrhizine/columbamine. Their markedly different retention times and relative fragment ion abundances suggested differences in the substitution pattern, potentially involving the position of the additional hydroxyl group and/or the arrangement of hydroxy- and methoxy-substituents on the protoberberine scaffold. Feature **A4** was therefore tentatively annotated as a hydroxyjatrorrhizine/hydroxycolumbamine isomer.

Feature **A7** was detected as a molecular cation at m/z 500.20 (Rt = 4.08 min), corresponding to the elemental composition $[C_{26}H_{30}NO_9]^+$. Collision-induced dissociation generated a prominent product ion at m/z 338.14 through loss of 162.05 Da, while the spectrum additionally contained the characteristic jatrorrhizine/columbamine-derived ions at m/z 323/322, 308/307, 294, 280/279, and 265. The mass difference between the precursor and the product ion at m/z 338.14 was 162.05 Da, corresponding to the composition $C_6H_{10}O_5$ and consistent with loss of a hexose residue. Together with its substantially shorter retention time relative to compounds **A10** and **A11**, this fragmentation behavior supported assignment of feature **A7** as an *O*-hexoside of a jatrorrhizine/columbamine-type protoberberine alkaloid. The identity of the hexose and the position of glycosylation could not be determined from the MS/MS data; therefore, feature **A7** was conservatively annotated as a jatrorrhizine/columbamine *O*-hexoside. Feature **A9** was detected as a molecular cation at m/z 534.2130 (Rt = 5.77 min), corresponding to the elemental composition $[C_{30}H_{32}NO_8]^+$. CID generated a prominent product ion at m/z 338.14, which subsequently exhibited the characteristic fragmentation pattern of the jatrorrhizine/columbamine-type core. The mass difference between the precursor and the m/z 338.14 ion was 196.07 Da, corresponding to the neutral loss of $C_{10}H_{12}O_4$. Thus, feature **A9** was interpreted as a modified jatrorrhizine/columbamine-type protoberberine bearing a $C_{10}H_{12}O_4$-derived substituent.

Feature **A3** was detected as a molecular cation at m/z 370.13, corresponding to the elemental composition $[C_{20}H_{20}NO_6]^+$. Its composition contained one additional oxygen atom relative to features **A4** and **A8** and two additional oxygen atoms relative to the jatrorrhizine/columbamine isomers. Notably, its major product ions at m/z 355.11, 312.09, and 284.09 were shifted by 16 Da relative to the corresponding ions at m/z 339.11, 296.09, and 268.09 in the spectrum of **A4**, indicating retention of the additional oxygen atom throughout this fragmentation series and strongly supporting a close structural relationship between the two metabolites. This closely homologous fragmentation behavior indicated that feature **A3** represented an additionally oxygenated analogue of the hydroxyjatrorrhizine/hydroxycolumbamine-type alkaloid represented by **A4**. Dihydroxyjatrorrhizine/dihydroxycolumbamine-type protoberberines with the same elemental composition have previously been reported from *Phellodendron* species [34]. Feature **A3** was therefore tentatively annotated as dihydroxyjatrorrhizine/dihydroxycolumbamine.

Isomeric features **A12** and **A13**, constituting molecular cluster P10, were detected at comparable relative abundances in both the root and aerial-part extracts. Both metabolites were observed as intrinsically doubly charged molecular cations at m/z 337.13, consistent with the ion formula $[C_{40}H_{38}N_2O_8]^{2+}$. CID produced an extensive series of doubly charged product ions arising from losses of $CH_3^{\bullet}$, CH_4, CH_3OH, CH_4 + CO and $2CH_3^{\bullet}$ + CO. This dissociation pattern was consistent with the characteristic fragmentation behavior of highly conjugated methoxylated quaternary protoberberine systems. The elemental composition corresponds formally to two jatrorrhizine/columbamine-type molecular cations joined with the net loss of 2H. Accordingly, features **A12** and **A13** were tentatively annotated as bisjatrorrhizine-type dimeric quaternary protoberberine alkaloids rather than bisbenzylisoquinoline alkaloids. The occurrence of two chromatographically resolved isomers may reflect alternative coupling regiochemistry and/or different combinations of jatrorrhizine- and columbamine-type subunits.

Several additional isoquinoline alkaloids occurred as singleton nodes. Feature **A6** (m/z 330.17, Rt = 3.78 min) was tentatively annotated as reticuline. Its MS/MS spectrum was dominated by the diagnostic product ions at m/z 192.10 and 137.06, arising from cleavage of the benzylisoquinoline skeleton, together with the fragment at m/z 299.13 corresponding to loss of CH_3NH_2. This fragmentation pattern closely matched that reported for reticuline [30]. Feature **A1** (m/z 462.21, Rt = 2.73 min) was tentatively assigned to a glycosylated benzyltetrahydroisoquinoline alkaloid. CID generated a prominent product ion at m/z 300.16 through neutral loss of a $C_6H_{10}O_5$ unit, consistent with cleavage of an *O*-linked hexose residue. Further fragmentation yielded the fragment at m/z 269.12, corresponding to loss of CH_3NH_2, a characteristic dissociation pathway of *N*-methylated benzyltetrahydroisoquinoline alkaloids [30]. Additional product ions at m/z 237.09, 209.10, 197.10, and 107.05 further supported a methoxylated benzyltetrahydroisoquinoline aglycone. Notably, an alkaloid exhibiting the same precursor ion and closely corresponding fragmentation series has previously been annotated as 7-methoxy-2-methylhigenamine-4′-*O*-glucoside/6-*O*-glucoside [35]. Feature **A1** was therefore tentatively annotated as a 7-methoxy-2-methylhigenamine *O*-hexoside; however, related positional isomers cannot be excluded. Feature **A2** (m/z 490.2067, Rt = 3.25 min) was tentatively assigned to a glycosylated aporphine alkaloid. Tandem MS initially produced the ion at m/z 459.17 through elimination of methylamine, followed by loss of a hexose residue to yield the abundant product ion at m/z 297.11. Further dissociation generated the characteristic series through successive losses of CH_3OH and CO. This fragmentation closely resembles that reported for *N*-methylated aporphine alkaloids such as boldine [28]. Although compounds with the same precursor composition have previously been annotated as 11-*O*-glucosyl-norisocorydine isomers, these metabolites predominantly underwent direct loss of hexose to form the protonated norisocorydine aglycone at m/z 328.15 [36]. The absence of this ion and the prominent methylamine loss observed for feature **A2** instead supports an *N*-methylated aporphine aglycone. Feature **A2** was therefore annotated as an *O*-hexoside of an *N*-methylated boldine/corytuberine-type aporphine.

In total, 14 alkaloid-related features were putatively annotated, encompassing several major structural branches of benzylisoquinoline alkaloid metabolism. The largest group comprised eight monomeric protoberberine-related metabolites, including jatrorrhizine/columbamine isomers, palmatine, their oxygenated and glycosylated derivatives, and a putative $C_{10}H_{12}O_4$-conjugated analogue. Two additional features were assigned to bisjatrorrhizine-type dimeric protoberberines, whereas the remaining metabolites included two aporphine alkaloids, represented by magnoflorine and a boldine/corytuberine-type *O*-hexoside, and two benzylisoquinoline-type alkaloids, reticuline and a 7-methoxy-2-methylhigenamine-type *O*-hexoside. Thus, the annotated alkaloid profile comprised not

only the abundant classical quaternary protoberberines but also oxygenated, glycosylated, conjugated, and dimeric derivatives.

The relative distribution of the annotated alkaloids revealed marked differences between the root and aerial-part extracts of *P. dubium*. The summed LC-MS signal of the annotated alkaloid features was approximately 2.7-fold higher in the root extract; however, this difference was largely attributable to magnoflorine (**A5**), which accounted for approximately 83% of the summed alkaloid-related LC-MS signal in roots. In contrast, the summed signal of the annotated alkaloid-related features in the aerial-part extract was dominated by the two jatrorrhizine/columbamine isomers (**A10** and **A11**), which together represented approximately 67% of the summed alkaloid signal in aerial parts. Several related metabolites were also strongly enriched in the aerial parts, including palmatine (**A14**), 13-hydroxyjatrorrhizine/13-hydroxycolumbamine (**A8**), and reticuline (**A6**). Conversely, oxygenated and conjugated protoberberine derivatives **A3**, **A4**, **A7**, **A9**, and the boldine/corytuberine-type *O*-hexoside **A2** showed higher LC-MS signals in the root extract. The two bisjatrorrhizine-type dimeric protoberberines (**A12** and **A13**) showed comparable LC-MS signals in the two parts, indicating substantially similar relative signals in the two extracts. At the structural-class level, the two organs exhibited contrasting alkaloid profiles. Aporphine-type alkaloids accounted for approximately 82.7% of the summed alkaloid signal in the roots but only 4.3% in the aerial parts, primarily because of the strong accumulation of magnoflorine. Conversely, monomeric protoberberine-related metabolites represented approximately 72.2% of the alkaloid signal in the aerial parts but only 9.1% in the roots.

3.2. Triterpene Glycosides

Feature-based molecular networking of the negative-ion MS/MS data revealed a prominent molecular family dominated by features tentatively assigned as triterpene glycosides (saponins). Molecular cluster N5 comprised 88 interconnected nodes, consistent with extensive structural diversity within this metabolite class (Figure 2). The relative LC-MS signals of individual features differed markedly between roots and aerial parts, indicating marked differences in saponin profiles between the two extracts.

Table 2. Putative structural composition of triterpene saponins detected in *P. dubium* by LC-HRMS/MS [a].

ID	Rt, min	$[M + HCOO]^-$ Meas., m/z	Neutral Molecular Formula	Assigned R Neutral Loss	Putative R_1 Neutral Loss	Glycan Composition	Neutral Aglycone Formula
G1	7.33	1121.5343	$C_{52}H_{84}O_{23}$	C_5H_8O		Pent-Hex-Hex-	$C_{30}H_{48}O_8$
G2	7.48	1121.5344	$C_{52}H_{84}O_{23}$	C_5H_8O		Pent-Hex-Hex-	$C_{30}H_{48}O_8$
G3	8.13	1091.5228	$C_{51}H_{82}O_{22}$	C_5H_8O		Pent-Hex-Pent-	$C_{30}H_{48}O_8$
G4	8.29	1091.5236	$C_{51}H_{82}O_{22}$	C_5H_8O		Pent-Hex-Pent-	$C_{30}H_{48}O_8$
G5	9.22	1179.5382	$C_{54}H_{86}O_{25}$		$C_7H_{12}O_4$	Pent-Hex-Hex-	$C_{30}H_{46}O_7$
G6	9.99	1221.5857	$C_{57}H_{92}O_{25}$	C_5H_8O	$C_5H_{10}O_3$	Pent-Hex-Hex-	$C_{30}H_{46}O_7$
G7	10.17	1149.5291	$C_{53}H_{84}O_{24}$		$C_7H_{12}O_4$	Pent-Hex-Pent-	$C_{30}H_{46}O_7$
G8	10.25	1221.5855	$C_{57}H_{92}O_{25}$	C_5H_8O	$C_5H_{10}O_3$	Pent-Hex-Hex-	$C_{30}H_{46}O_7$
G9	10.85	1191.5759	$C_{56}H_{90}O_{24}$	C_5H_8O	$C_5H_{10}O_3$	Pent-Hex-Pent-	$C_{30}H_{46}O_7$
G10	11.36	1191.6119	$C_{57}H_{94}O_{23}$	C_5H_8O	$C_5H_{10}O_2$	Pent-Hex-Hex-	$C_{30}H_{48}O_6$
G11	11.41	1207.5711	$C_{56}H_{90}O_{25}$		$C_9H_{16}O_4$	Pent-Hex-Hex-	$C_{30}H_{46}O_7$
G12	11.56	1249.5822	$C_{58}H_{92}O_{26}$	C_5H_8O	$C_7H_{12}O_4$	Pent-Hex-Hex-	$C_{29}H_{44}O_7$
G13	11.82	1249.5812	$C_{58}H_{92}O_{26}$	C_5H_8O	$C_6H_{10}O_4$	Pent-Hex-Hex-	$C_{30}H_{46}O_7$
G14	12.09	1191.5771	$C_{56}H_{90}O_{24}$		$C_9H_{16}O_4$	Pent-Hex-Hex-	$C_{30}H_{46}O_6$
G15	12.18	1233.5868	$C_{58}H_{92}O_{25}$	C_5H_8O	$C_6H_{10}O_4$	Pent-Hex-Hex-	$C_{30}H_{46}O_6$

Table 2. *Cont.*

ID	Rt, min	[M + HCOO]$^-$ Meas., *m*/*z*	Neutral Molecular Formula	Assigned R Neutral Loss	Putative R_1 Neutral Loss	Glycan Composition	Neutral Aglycone Formula
G16	12.33	1177.5608	$C_{55}H_{88}O_{24}$		$C_9H_{16}O_4$	Pent-Hex-Pent-	$C_{30}H_{46}O_7$
G17	12.34	1219.5714	$C_{57}H_{90}O_{25}$	C_5H_8O	$C_7H_{12}O_4$	Pent-Hex-Pent-	$C_{29}H_{44}O_7$
G18	12.45	1263.5975	$C_{59}H_{94}O_{26}$	C_5H_8O	$C_7H_{12}O_4$	Pent-Hex-Hex-	$C_{30}H_{46}O_7$
G19	12.50	1175.5810	$C_{56}H_{90}O_{23}$	C_5H_8O	$C_4H_8O_2$	Pent-Hex-Hex-	$C_{30}H_{46}O_6$
G20	12.57	1219.5713	$C_{57}H_{90}O_{25}$	C_5H_8O	$C_6H_{10}O_4$	Pent-Hex-Pent-	$C_{30}H_{46}O_7$
G21	12.63	1205.5917	$C_{57}H_{92}O_{24}$	C_5H_8O	$C_5H_{10}O_2$	Pent-Hex-Hex-	$C_{30}H_{46}O_7$
G22	12.75	1263.5975	$C_{59}H_{94}O_{26}$	C_5H_8O	$C_7H_{12}O_4$	Pent-Hex-Hex-	$C_{30}H_{46}O_7$
G23	12.98	1263.5962	$C_{59}H_{94}O_{26}$	C_5H_8O	$C_7H_{12}O_4$	Pent-Hex-Hex-	$C_{30}H_{46}O_7$
G24	13.14	1247.6032	$C_{59}H_{94}O_{25}$	C_5H_8O	$C_7H_{12}O_4$	Pent-Hex-Hex-	$C_{30}H_{46}O_6$
G25	13.23	1233.5871	$C_{58}H_{92}O_{25}$	C_5H_8O	$C_7H_{12}O_4$	Pent-Hex-Pent-	$C_{30}H_{46}O_7$
G26	13.29	1189.5973	$C_{57}H_{92}O_{23}$	C_5H_8O	$C_5H_{10}O_2$	Pent-Hex-Hex-	$C_{30}H_{46}O_6$
G27	13.42	1247.6023	$C_{59}H_{94}O_{25}$	C_5H_8O	$C_7H_{12}O_4$	Pent-Hex-Hex-	$C_{30}H_{46}O_6$
G28	13.45	1175.5819	$C_{56}H_{90}O_{23}$	C_5H_8O	$C_5H_{10}O_2$	Pent-Hex-Pent-	$C_{30}H_{46}O_7$
G29	13.48	1189.5970	$C_{57}H_{92}O_{23}$	C_5H_8O	$C_5H_{10}O_2$	Pent-Hex-Hex-	$C_{30}H_{46}O_6$
G30	13.54	1233.5868	$C_{58}H_{92}O_{25}$	C_5H_8O	$C_7H_{12}O_4$	Pent-Hex-Pent-	$C_{30}H_{46}O_7$
G31	13.71	1115.5617	$C_{54}H_{86}O_{21}$	C_5H_8O	$C_7H_{12}O_4$	Hex-Hex-	$C_{30}H_{46}O_6$
G32	13.75	1101.5457	$C_{53}H_{84}O_{21}$	C_5H_8O	$C_7H_{12}O_4$	Hex-Pent-	$C_{30}H_{46}O_7$
G33	13.85	1277.6123	$C_{60}H_{96}O_{26}$	C_5H_8O	$C_9H_{16}O_4$	Pent-Hex-Hex-	$C_{29}H_{44}O_7$
G34	13.94	1115.5616	$C_{54}H_{86}O_{21}$	C_5H_8O	$C_7H_{12}O_4$	Hex-Hex-	$C_{30}H_{46}O_6$
G35	14.02	1233.5856	$C_{58}H_{92}O_{25}$	C_5H_8O	$C_7H_{12}O_4$	Pent-Hex-Pent-	$C_{30}H_{46}O_7$
G36	14.08	1101.5461	$C_{53}H_{84}O_{21}$	C_5H_8O	$C_7H_{12}O_4$	Hex-Pent-	$C_{30}H_{46}O_7$
G37	14.21	1277.6127	$C_{60}H_{96}O_{26}$	C_5H_8O	$C_8H_{14}O_4$	Pent-Hex-Hex-	$C_{30}H_{46}O_7$
G38	14.58	1261.6187	$C_{60}H_{96}O_{25}$	C_5H_8O	$C_8H_{14}O_4$	Pent-Hex-Hex-	$C_{30}H_{46}O_6$
G39	14.67	1247.6023	$C_{59}H_{94}O_{25}$	C_5H_8O	$C_9H_{16}O_4$	Pent-Hex-Pent-	$C_{29}H_{44}O_7$
G40	14.75	1291.6281	$C_{61}H_{98}O_{26}$	C_5H_8O	$C_9H_{16}O_4$	Pent-Hex-Hex-	$C_{30}H_{46}O_7$
G41	14.86	1261.6188	$C_{60}H_{96}O_{25}$	C_5H_8O	$C_8H_{14}O_4$	Pent-Hex-Hex-	$C_{30}H_{46}O_6$
G42	14.97	1247.6032	$C_{59}H_{94}O_{25}$	C_5H_8O	$C_8H_{14}O_4$	Pent-Hex-Pent-	$C_{30}H_{46}O_7$
G43	15.13	1291.6277	$C_{61}H_{98}O_{26}$	C_5H_8O	$C_9H_{16}O_4$	Pent-Hex-Hex-	$C_{30}H_{46}O_7$
G44	15.29	1115.5623	$C_{54}H_{86}O_{21}$	C_5H_8O	$C_8H_{14}O_4$	Hex-Pent-	$C_{30}H_{46}O_7$
G45	15.43	1129.5773	$C_{55}H_{88}O_{21}$	C_5H_8O	$C_8H_{14}O_4$	Hex-Hex-	$C_{30}H_{46}O_6$
G46	15.47	1275.6348	$C_{61}H_{98}O_{25}$	C_5H_8O	$C_9H_{16}O_4$	Pent-Hex-Hex-	$C_{30}H_{46}O_6$
G47	15.56	1261.6189	$C_{60}H_{96}O_{25}$	C_5H_8O	$C_9H_{16}O_4$	Pent-Hex-Pent-	$C_{30}H_{46}O_7$
G48	15.59	1115.5615	$C_{54}H_{86}O_{21}$	C_5H_8O	$C_8H_{14}O_4$	Hex-Pent-	$C_{30}H_{46}O_7$
G49	15.64	1275.6339	$C_{61}H_{98}O_{25}$	C_5H_8O	$C_9H_{16}O_4$	Pent-Hex-Hex-	$C_{30}H_{46}O_6$
G50	15.75	1305.6440	$C_{62}H_{100}O_{26}$	C_5H_8O	$C_{10}H_{18}O_4$	Pent-Hex-Hex-	$C_{30}H_{46}O_7$
G51	15.83	1275.6344	$C_{61}H_{98}O_{25}$	C_5H_8O	$C_9H_{16}O_4$	Pent-Hex-Hex-	$C_{30}H_{46}O_6$
G52	15.94	1261.6176	$C_{60}H_{96}O_{25}$	C_5H_8O	$C_9H_{16}O_4$	Pent-Hex-Pent-	$C_{30}H_{46}O_7$
G53	16.10	1305.6438	$C_{62}H_{100}O_{26}$	C_5H_8O	$C_{10}H_{18}O_4$	Pent-Hex-Hex-	$C_{30}H_{46}O_7$
G54	16.10	1261.6176	$C_{60}H_{96}O_{25}$	C_5H_8O	$C_9H_{16}O_4$	Pent-Hex-Pent-	$C_{30}H_{46}O_7$
G55	16.17	1129.5769	$C_{55}H_{88}O_{21}$	C_5H_8O	$C_9H_{16}O_4$	Hex-Pent-	$C_{30}H_{46}O_7$
G56	16.32	1129.5767	$C_{55}H_{88}O_{21}$	C_5H_8O	$C_9H_{16}O_4$	Hex-Pent-	$C_{30}H_{46}O_7$
G57	16.57	1129.5769	$C_{55}H_{88}O_{21}$	C_5H_8O	$C_9H_{16}O_4$	Hex-Pent-	$C_{30}H_{46}O_7$
G58	16.57	1275.6338	$C_{61}H_{98}O_{25}$	C_5H_8O	$C_{10}H_{18}O_4$	Pent-Hex-Pent-	$C_{30}H_{46}O_7$
G59	16.65	1289.6497	$C_{62}H_{100}O_{25}$	C_5H_8O	$C_{10}H_{18}O_4$	Pent-Hex-Hex-	$C_{30}H_{46}O_6$
G60	16.85	1289.6497	$C_{62}H_{100}O_{25}$	C_5H_8O	$C_{10}H_{18}O_4$	Pent-Hex-Hex-	$C_{30}H_{46}O_6$
G61	16.92	1275.6335	$C_{61}H_{98}O_{25}$	C_5H_8O	$C_{10}H_{18}O_4$	Pent-Hex-Pent-	$C_{30}H_{46}O_7$

[a] All saponin annotations were classified as MSI Level 3.

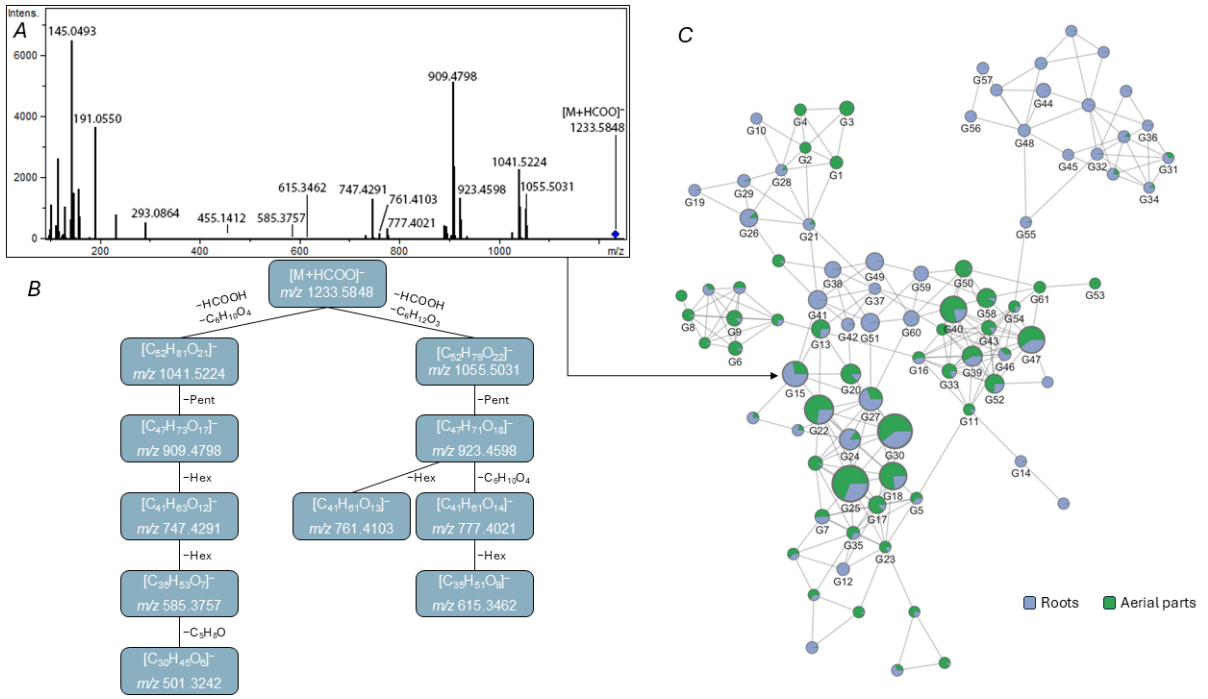


Figure 2. MS/MS fragmentation and molecular-network context of representative triterpene glycoside **G15** from *P. dubium*. (**A**) Negative-ion MS/MS spectrum of **G15**. (**B**) Proposed fragmentation pathway of **G15** showing the major product ions. (**C**) Feature-based molecular network of molecular cluster N5, comprising structurally related saponins. Nodes represent individual LC-MS/MS features, edges indicate spectral similarity, and pie-chart sectors show the relative contribution of roots (blue) and aerial parts (green) to the corresponding feature signal. Labeled nodes correspond to retained saponin-related features listed in Tables 2 and S2; unlabeled nodes represent additional spectrally related features not included in the detailed annotation.

Structural annotation of the saponins was based on accurate-mass measurements and characteristic fragmentation patterns observed in positive- and negative-ion MS/MS spectra. The detected product ions and neutral losses were used to infer the elemental compositions of glycan moieties, aglycone-related fragments, and additional substituents. However, the available MS/MS data do not allow unambiguous determination of individual monosaccharide identities, glycosidic linkages, aglycone carbon skeletons, or substitution positions. Therefore, the structural assignments discussed below should be regarded as tentative, and the proposed structures represent possible interpretations of the experimental data supported by literature evidence.

Most features within this cluster exhibited precursor ions in the m/z 1050–1250 range and were detected predominantly as formate adducts, $[M + HCOO]^-$. Formation of formate- or acetate-adducted anions is well documented for neutral oligosaccharides and triterpene saponins and provides an efficient pathway for their detection by negative-mode ESI when direct deprotonation is unfavorable [37,38]. The predominance of $[M + HCOO]^-$ ions over $[M - H]^-$ ions may suggest a relatively low tendency of these glycosides to undergo direct deprotonation under the applied ionization conditions. This observation is consistent with the hypothesis that the major saponins lack free carboxyl groups or contain carboxyl groups involved in ester linkages. However, formate adduct formation is also influenced by the molecular structure and ionization conditions and cannot be used alone to establish the presence, absence, or esterification state of carboxyl groups. Therefore, the proposed neutral character of these glycosides should be regarded as a tentative structural interpretation rather than a definitive conclusion. Although the negative-ion product ion spectra were generally of low intensity and contained a relatively limited number of diagnostic ions, their combined

interpretation with the corresponding positive-ion spectra supported tentative structural annotation. Sequential glycosidic cleavages and the resulting neutral losses provided information on the number and nominal composition of monosaccharide residues, whereas complementary product-ion series facilitated assignment of the elemental compositions of the aglycone-related and non-carbohydrate substituent fragments [37,39].

For example, the product ion spectrum of feature **G15**, one of the most abundant putative saponin-related components in the root extract ($C_{58}H_{92}O_{25}$, m/z 1233.58 $[M + HCOO]^-$, Rt 12.18 min), exhibited a characteristic fragmentation pattern in the negative-ion mode. The product-ion spectrum contained a prominent ion at m/z 1041.52 formed by initial elimination of formic acid from the $[M + HCOO]^-$ precursor followed by a neutral loss of 146.06 Da ($C_6H_{10}O_4$). The occurrence of the same $C_6H_{10}O_4$ moiety was further supported by an abundant low-mass product ion at m/z 145.05 $[C_6H_9O_4]^-$. In the product ion spectrum of the corresponding $[M + H]^+$ ion at m/z 1189.60, aglycone-related ions were observed at m/z 631.39 $[C_{36}H_{55}O_9]^+$ and 485.33 $[C_{30}H_{45}O_5]^+$. Their elemental compositions differed by $C_6H_{10}O_4$, indicating that this moiety was retained in an aglycone-containing fragment, supporting its association with the triterpene aglycone. The negative fragment ion at m/z 1041.52 subsequently generated a series of Y-type product ions [40] at m/z 909.48 $[M - H - C_6H_{10}O_4 - Pent]^-$, 747.43 $[M - H - C_6H_{10}O_4 - Pent - Hex]^-$, and 585.38 $[M - H - C_6H_{10}O_4 - Pent - 2Hex]^-$. The complementary B- and Y-type product-ion series supported a glycan composition of Pent + 2Hex. The observed fragmentation was consistent with a linear Pent–Hex–Hex sequence containing a terminal pentose residue. This assignment was independently supported by a complementary series of carbohydrate-retaining B-type ions at m/z 131.03 $[Pent]^-$, 293.09 $[Pent + Hex]^-$, and 455.14 $[Pent + 2Hex]^-$.

The aglycone-related product ion at m/z 585.38 $[C_{35}H_{53}O_7]^-$, generated after elimination of the oligosaccharide chain and the $C_6H_{10}O_4$ substituent, subsequently yielded a low-abundance ion at m/z 501.32 $[C_{30}H_{45}O_6]^-$ through a neutral loss of C_5H_8O. The elemental compositions and accurate masses of these products were consistent with a highly oxygenated C_{30} triterpene aglycone having the molecular formula $C_{30}H_{46}O_6$. Complementary evidence for the C_5-derived substituent was obtained in the positive product ion spectrum of $[M + H]^+$ precursor. Two related aglycone-derived series were observed at m/z 587.39, 569.38, and 551.37, differing by successive losses of H_2O, and at m/z 485.33, 467.32, and 449.31. The transition from m/z 587.39 to m/z 485.33 corresponded to a neutral loss of 102.07 Da ($C_5H_{10}O_2$). Notably, the latter product is consistent with the dehydrated protonated form of the same $C_{30}H_{46}O_6$ aglycone inferred from the negative-ion spectrum. Losses of $C_5H_{10}O_2$ have previously been associated with cleavage of C_5-acyl substituents, including methylbutyryl- and isovaleryl-derived groups, in acylated triterpene saponins [41]. Taken together, the complementary fragmentation pathways strongly support the presence of a C_5-acyl substituent derived from a saturated $C_5H_{10}O_2$ monocarboxylic acid and contributing a net elemental increment of C_5H_8O upon esterification of the aglycone.

Furthermore, an additional prominent fragmentation pathway was observed for compound **G15**. Following dissociation of the formate adduct, a neutral loss of 132.08 Da ($C_6H_{12}O_3$) generated the product ion at m/z 1055.50. The elemental composition $C_6H_{12}O_3$ can formally be expressed as $C_5H_8O + H_2O + CH_2O$ and may therefore arise from a composite fragmentation process involving the C_5-acylated aglycone rather than from cleavage of an independently attached $C_6H_{12}O_3$ substituent. This interpretation was further supported by the fragmentation behavior across the molecular family: compounds lacking the characteristic $C_6H_{12}O_3$ loss also lacked the C_{35} aglycone-related product ions associated with the C_5-acylated aglycone. Thus, within this saponin family, the recurrent $C_6H_{12}O_3$ loss appears to be specifically associated with fragmentation of the C_5-acylated aglycone motif. Subsequent loss of a pentose residue from the $[M - H - C_6H_{12}O_3]^-$ generated the

product ion at m/z 923.46. This ion underwent two competing fragmentation pathways. Elimination of the $C_6H_{10}O_4$ moiety yielded the product ion at m/z 777.40, which subsequently generated m/z 615.35 through loss of hexose residue. Alternatively, direct loss of Hex from m/z 923.46 produced the ion at m/z 761.41. Taken together, the complementary negative- and positive-ion tandem MS data support the assignment of compound **G15** as a highly oxygenated C_{30}-triterpene saponin. The fragmentation patterns are consistent with an oligosaccharide moiety composed of one pentose and two hexose residues. They also suggest the presence of two aglycone-associated structural motifs corresponding to the elemental compositions $C_6H_{10}O_4$ and C_5H_8O. Although the overall structural model was supported by the combined MS/MS evidence, the exact attachment sites and the detailed fragmentation mechanism remain tentative.

An alternative interpretation of the $C_6H_{10}O_4$ neutral loss should also be considered. This elemental composition corresponds to a 6-deoxyhexose residue, such as rhamnose or fucose, and the product ion at m/z 145.05 $[C_6H_9O_4]^-$ is compatible with a deoxyhexose-derived fragment. Furthermore, retention of the $C_6H_{10}O_4$ unit in aglycone-containing product ions does not exclude its attachment as a separate glycosidic substituent, potentially through an ester linkage. Therefore, the available MS/MS data do not allow an unambiguous distinction between a deoxyhexose residue and a non-carbohydrate substituent for **G15** and related features.

Isotope- and adduct-related nodes, in-source fragments, and features lacking sufficient structural information were excluded from detailed annotation. The remaining 61 LC-MS features were putatively annotated as triterpene saponins (Tables 2 and S2). These components corresponded to 26 distinct molecular formulas and 38 distinct combinations of the assigned aglycone, carbohydrate moiety, and non-carbohydrate substituents. Eighteen of these structural combinations were represented by two or more chromatographically resolved isomers, indicating considerable positional and/or stereochemical diversity within detected saponins. Despite this structural heterogeneity, the annotated saponins could be accommodated within a common framework comprising a triterpene aglycone, a di- or trisaccharide moiety, and a variable oxygenated substituent; most components additionally contained a recurrent C_5-derived residue with the net elemental composition C_5H_8O.

Five aglycone elemental compositions were inferred from the MS/MS data: $C_{30}H_{46}O_6$, $C_{30}H_{46}O_7$, $C_{30}H_{48}O_8$, $C_{29}H_{44}O_7$, and $C_{30}H_{48}O_6$. The two predominant compositions, $C_{30}H_{46}O_6$ and $C_{30}H_{46}O_7$, are consistent with highly oxygenated pentacyclic triterpenoid aglycones and differ by a single oxygen atom. Although several structurally distinct sapogenins may correspond to these elemental compositions, the available MS/MS data do not allow their individual carbon skeletons or functional group arrangements to be determined. Considering the observed predominance of formate adducts and structural precedents among triterpene saponins from other representatives of Berberidaceae, we considered a hypothetical oleanane-type model without free carboxyl groups as one possible structural interpretation (Figure 3). This model is compatible with the observed elemental compositions and fragmentation behavior but is not uniquely supported by the present data. The minor $C_{29}H_{44}O_7$ family may represent a nortriterpenoid analogue of the $C_{30}H_{46}O_7$ series, whereas $C_{30}H_{48}O_6$ differs from $C_{30}H_{46}O_6$ by two hydrogen atoms and may represent a more reduced analogue. The R- and R_1-associated moieties underwent relatively facile and largely independent losses from aglycone-derived ions. A recurrent composite neutral loss corresponding to $C_5H_8O + H_2O + CH_2O$ was also observed. Together, these fragmentation patterns may be compatible with a proximal arrangement of the substituents on the triterpenoid scaffold. A vicinal placement at C-21 and C-22 is therefore proposed as one plausible structural model, although these positions cannot be established unambiguously from the present data. The additional oxygen atom distinguishing the $C_{30}H_{46}O_7$ family

from $C_{30}H_{46}O_6$ may correspond to an additional hydroxy group; in the proposed model, this functionality is tentatively placed at C-16 on the basis of structural precedents among hydroxylated oleanane sapogenins in Berberidaceae [42]. Likewise, the positions of the carbonyl functionality and the R and R_1 substituents shown in Figure 3 should be regarded as hypothetical and require confirmation by isolation and NMR analysis. The carbohydrate moieties were tentatively assigned as Pent–Hex–Hex in 33 metabolites, Pent–Hex–Pent in 18 metabolites, Hex–Pent in seven metabolites, and Hex–Hex in three metabolites.

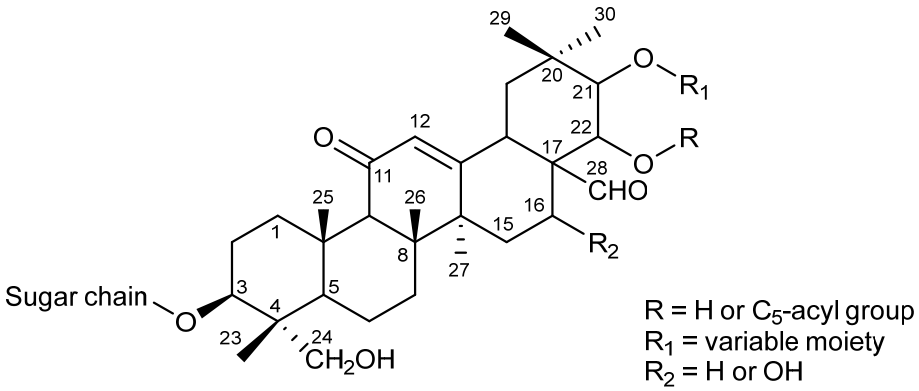


Figure 3. Hypothetical oleanane-type structural model illustrating a possible arrangement of the major structural elements of $C_{30}H_{46}O_6$ and $C_{30}H_{46}O_7$ aglycones of triterpene glycosides detected in *P. dubium*.

The variable R_1 moiety represented one of the major sources of structural diversity within the detected saponin family. Most components belonged to a homologous series characterized by neutral losses with elemental compositions ranging from $C_6H_{10}O_4$ to $C_{10}H_{18}O_4$. Other features exhibited losses corresponding to shorter R_1-related moieties, including $C_4H_8O_2$, $C_5H_{10}O_2$, and $C_5H_{10}O_3$, which occurred less frequently. The most numerous groups were those containing $C_7H_{12}O_4$ and $C_9H_{16}O_4$, each comprising 16 chromatographic components, followed by $C_8H_{14}O_4$ with seven components, and $C_{10}H_{18}O_4$ with six components (Tables 2 and S2). Collectively, the $C_6H_{10}O_4$–$C_{10}H_{18}O_4$ homologous series accounted for 48 of the 61 annotated saponins and approximately 90% of the summed saponin signal in both plant organs. Notably, the compositions $C_6H_{10}O_4$, $C_7H_{12}O_4$, $C_8H_{14}O_4$, $C_9H_{16}O_4$, and $C_{10}H_{18}O_4$ follow the general formula $C_nH_{2n-2}O_4$ and differ successively by CH_2. Retention of the R_1 moiety in aglycone-containing product ions indicates that these substituents are directly associated with the non-carbohydrate portion of the saponins. The lower members of the series also admit carbohydrate-based interpretations: $C_6H_{10}O_4$ corresponds to a deoxyhexose residue, whereas $C_7H_{12}O_4$ is compatible with an *O*-methylated deoxyhexose residue. Although the extended homologous series up to $C_{10}H_{18}O_4$ may favor a common non-carbohydrate structural motif, it does not provide definitive evidence for this assignment. Accordingly, the chemical identities, the mode and site of attachment could not be established from the present MS/MS data.

A C_5-derived acyl modification represented another recurrent structural feature of this saponin family. Fifty-six of the 61 annotated components contained the corresponding C_5H_8O residue, whereas the remaining five lacked this modification and were assigned as putative non-C_5-acylated counterparts. The notation C_5H_8O refers to the net elemental increment introduced upon esterification of a saponin hydroxyl group with a saturated $C_5H_{10}O_2$ monocarboxylic acid. Several constitutional isomers are compatible with the inferred precursor-acid composition $C_5H_{10}O_2$, including pentanoic, 2-methylbutanoic, 3-methylbutanoic, and 2,2-dimethylpropanoic acids. Among

these possibilities, 2-methylbutanoyl and 3-methylbutanoyl (isovaleryl) substituents have direct precedents among structurally characterized triterpene saponins [43–45].

Semi-quantitative analysis revealed pronounced differences in the triterpene saponin profiles of the pooled root and aerial-part extracts. Despite the broadly comparable total glycoside signal in the roots and aerial parts, the relative contributions of individual structural families differed markedly between the two organs. Thirty of the 61 components showed higher LC-MS signals in the roots, whereas 31 were more abundant in the aerial parts. The most pronounced difference was associated with the assigned aglycone composition. Saponins assigned to the $C_{30}H_{46}O_6$ aglycone family accounted for approximately 53% of the summed glycoside signal in the roots but only 7% in the aerial parts. In contrast, the more highly oxygenated $C_{30}H_{46}O_7$ family constituted 80% of the total glycoside signal in the aerial parts compared with 42% in the roots. Consequently, the $C_{30}H_{46}O_7/C_{30}H_{46}O_6$ signal ratio increased from approximately 0.8 in the roots to 12.1 in the aerial parts. The minor $C_{29}H_{44}O_7$ and $C_{30}H_{48}O_8$ families also showed higher relative LC-MS signals in the aerial organs, whereas the single $C_{30}H_{48}O_6$-containing component was strongly root-enriched.

The composition of the carbohydrate moiety showed an equally clear relationship with organ distribution. Pent–Hex–Hex-containing saponins represented 66.2% of the summed saponin signal in the roots and 46.1% in the aerial parts, whereas Pent–Hex–Pent-containing compounds showed the opposite tendency, accounting for 27.0 and 53.7% of the respective profiles. The biggest difference was observed for the shorter disaccharide-containing saponins. Hex–Pent compounds contributed approximately 6% of the root saponin signal but less than 0.1% of that in the aerial parts. Hex–Hex-containing compounds were likewise root-enriched, although they represented only a minor fraction of the total profile. The variable R_1 moiety provided a further level of organ-dependent differentiation, although its effect was strongly dependent on the accompanying aglycone and carbohydrate structures. The two quantitatively predominant R_1 groups, $C_7H_{12}O_4$ and $C_9H_{16}O_4$, occurred at high abundance in both organs and accounted together for approximately 61% and 70% of the total glycoside signal in the roots and aerial parts, respectively. In contrast, the $C_8H_{14}O_4$-containing series displayed substantially higher relative signal in the root extract: its seven components represented approximately 15% of the total root saponin signal but less than 0.2% of the aerial-part signal. The opposite pattern was observed for the less common $C_5H_{10}O_3$-containing group, which was approximately 9.8-fold more abundant in the aerial parts than in the roots. The recurrent C_5-derived acyl modification was abundant in both organs. The 56 components containing the C_5H_8O residue accounted for 97.4% of the summed glycoside signal in the roots and 93.2% in the aerial parts, indicating that C_5-acylation is a general characteristic of the major saponin pool rather than an organ-specific modification. The five putatively deacylated analogues made a greater relative contribution in the aerial parts (6.8%) than in the roots (2.6%) and collectively showed an approximately threefold higher signal in aerial parts.

In addition to the major molecular family N5, several smaller molecular families were observed whose components were tentatively attributed to triterpene glycosides. Molecular families N6 (17 features), N12 (6 features), and N15 (4 features) contained deprotonated molecular ions, $[M - H]^-$, predominantly in the m/z 800–1100 range. The MS/MS spectra of most features showed neutral losses consistent with pentose and hexose residues, supporting the presence of glycosylated structures. However, the generally low precursor-ion intensities and poorly informative fragmentation patterns precluded more detailed structural interpretation of the components within these molecular families.

3.3. Flavonoids and Hydroxycinnamate-Related Metabolites

Seventeen features were putatively annotated in the negative-ion data, including six flavonoid glycosides, ten hydroxycinnamate derivatives, and quinic acid (Figure 4; Tables 3 and S3). Molecular cluster N10 was associated predominantly with flavonoid glycosides, six of which could be structurally annotated based on accurate-mass measurements and characteristic negative-ion fragmentation. Five components (features **F15**, **F9**, **F17**, **F11**, and **F13**) were assigned to kaempferol glycosides. Their MS/MS spectra contained the characteristic kaempferol-derived ions at *m*/*z* 285.04/284.03, 255.03, and 227.03 [46]. In most of these spectra, the radical aglycone ion $[Y_0 - H]^{-\bullet}$ at *m*/*z* 284.03 was more abundant than the conventional deprotonated aglycone ion Y_0 at *m*/*z* 285.04. Homolytic cleavage of the *O*-glycosidic bond with formation of a radical aglycone anion has previously been shown to be particularly favored for flavonol 3-*O*-glycosides in negative-ion CID, whereas corresponding glycosides substituted at other positions generally show a greater contribution from heterolytic cleavage yielding Y_0 [47,48]. Thus, the predominance of *m*/*z* 284 over *m*/*z* 285 was considered consistent with 3-*O*-glycosylation, although the glycosylation position was regarded as tentative in the absence of authentic standards.

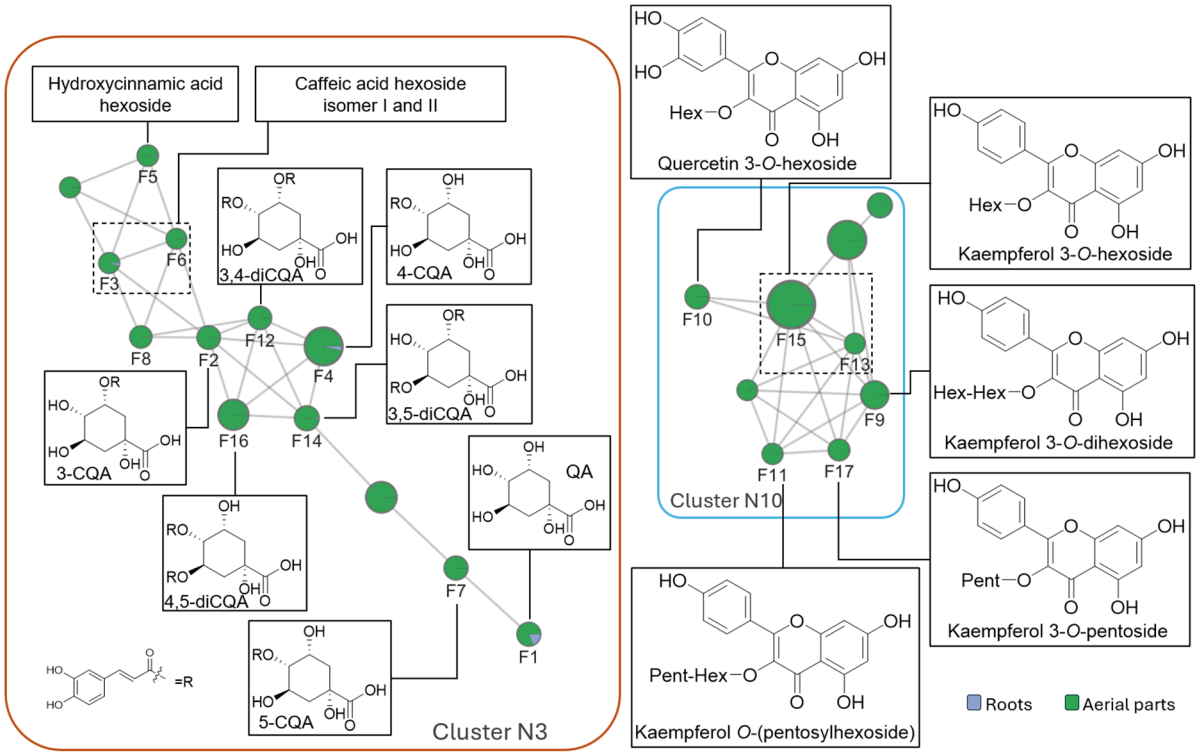


Figure 4. Feature-based molecular networks of flavonoid- and hydroxycinnamate-related features detected in the roots and aerial parts of *P. dubium* by negative-ion LC-MS/MS. Nodes represent individual LC-MS features, whereas edges connect features exhibiting similar MS/MS fragmentation patterns. Pie-chart sectors indicate the relative distribution of the LC-MS signal between root (blue) and aerial-part (green) extracts, and node size is proportional to the summed signal of the corresponding feature. Molecular cluster N3 comprises predominantly hydroxycinnamate-related metabolites, including mono- and dicaffeoylquinic acids, whereas cluster N10 is associated with flavonoid glycosides. Annotated features are labeled according to the IDs given in Table 3; additional nodes represent unannotated or ion-related features. CQA, caffeoylquinic acid; diCQA, dicaffeoylquinic acid; QA, quinic acid; Hex, hexose residue; Pent, pentose residue.

Table 3. Putatively annotated flavonoid, hydroxycinnamate, and related metabolites detected in *P. dubium* by negative-ion LC-HRMS/MS [a].

ID	Measured *m*/*z*	Rt (min)	Ion Formula	Putative Annotation
F1	191.0557	0.96	$[C_7H_{11}O_6]^-$	Quinic acid
F2	353.0867	2.72	$[C_{16}H_{17}O_9]^-$	3-*O*-Caffeoylquinic acid
F3	341.0864	3.09	$[C_{15}H_{17}O_9]^-$	Caffeic acid hexoside, isomer I
F4	353.0865	3.18	$[C_{16}H_{17}O_9]^-$	4-*O*-Caffeoylquinic acid
F5	325.0915	3.25	$[C_{15}H_{17}O_8]^-$	Hydroxycinnamic acid hexoside (putatively *p*-coumaric acid hexoside)
F6	341.0864	3.49	$[C_{15}H_{17}O_9]^-$	Caffeic acid hexoside, isomer II
F7	353.0866	3.55	$[C_{16}H_{17}O_9]^-$	5-*O*-Caffeoylquinic acid
F8	335.0761	3.75	$[C_{16}H_{15}O_8]^-$	Caffeoylshikimic acid
F9	609.1438	4.07	$[C_{27}H_{29}O_{16}]^-$	Kaempferol 3-*O*-dihexoside (putatively kaempferol 3-*O*-sophoroside)
F10	463.0867	4.61	$[C_{21}H_{19}O_{12}]^-$	Quercetin 3-*O*-hexoside (putatively isoquercitrin or hyperoside)
F11	579.1331	4.76	$[C_{26}H_{27}O_{15}]^-$	Kaempferol *O*-(pentosylhexoside) putatively kaempferol 3-O-sambubioside
F12	515.1177	4.92	$[C_{25}H_{23}O_{12}]^-$	3,4-Di-*O*-caffeoylquinic acid
F13	447.0915	5.03	$[C_{21}H_{19}O_{11}]^-$	Kaempferol 3-*O*-hexoside putatively astragalin or trifolin
F14	515.1181	5.18	$[C_{25}H_{23}O_{12}]^-$	3,5-Di-*O*-caffeoylquinic acid
F15	447.0923	5.24	$[C_{21}H_{19}O_{11}]^-$	Kaempferol 3-*O*-hexoside putatively astragalin or trifolin
F16	515.1185	5.51	$[C_{25}H_{23}O_{12}]^-$	4,5-Di-*O*-caffeoylquinic acid
F17	417.0814	5.69	$[C_{20}H_{17}O_{10}]^-$	Kaempferol 3-*O*-pentoside

[a] The annotations of features **F1**, **F2**, **F4**, **F7**, **F8**, **F9**, **F12**, **F14**, **F16** were classified as MSI Level 2, whereas all remaining annotations were classified as MSI Level 3.

The composition of the glycosyl moieties was inferred from the accurate masses of the precursor and product ions and from characteristic neutral losses. Isomeric features **F13** and **F15** exhibited a neutral loss of 162.05 Da, corresponding to a hexose residue, and were therefore annotated as putative kaempferol 3-*O*-hexosides. Their occurrence as two chromatographically resolved isomers is consistent with the presence of different hexose epimers; accordingly, kaempferol 3-*O*-glucoside (astragalin) and kaempferol 3-*O*-galactoside (trifolin) represent plausible candidate structures. Feature **F17** showed a corresponding neutral loss of 132.04 Da, characteristic of a pentose residue, and was annotated as putative kaempferol 3-*O*-pentoside. Components **F9** and **F11** showed a series of Y ions indicating the detachment of two monosaccharide residues—two hexoses in the case of **F9** and a pentose and a hexose in the case of **F11**. Feature **F9** was therefore annotated as kaempferol 3-*O*-dihexoside, with kaempferol 3-*O*-sophoroside considered the most plausible candidate structure. Feature **F11** underwent an overall neutral loss of 294.09 Da, corresponding to a combined pentose and hexose moiety, to yield the kaempferol aglycone at *m*/*z* 285.038. This component was consequently assigned as kaempferol 3-*O*-pentosylhexoside, with kaempferol *O*-sambubioside as a possible candidate.

The remaining annotated member of molecular family N10, feature **F10**, was assigned to a quercetin glycoside. Its $[M-H]^-$ precursor generated the aglycone-related ions at *m*/*z* 301.03 and 300.03 following a neutral loss of 162.05 Da, consistent with cleavage of a hexose residue. Subsequent fragmentation produced ions at *m*/*z* 271.02, 255.03, 243.03, 227.03, 215.03, 199.04, and 187.04, consistent with the fragmentation behavior of the quercetin aglycone [46]. As observed for kaempferol glycosides, the radical aglycone ion at *m*/*z* 300 was more intense than the even-electron ion at *m*/*z* 301, supporting a flavonol 3-*O*-glycoside structure [47,48]. Feature **F10** was therefore annotated as putative quercetin

3-*O*-hexoside, with quercetin 3-*O*-glucoside or quercetin 3-*O*-galactoside (hyperoside) representing possible candidate structures.

Molecular family N3 was dominated by hydroxycinnamic acid derivatives. Feature **F1** was annotated as quinic acid (QA) based on its accurate mass and characteristic negative ion fragmentation. Three chromatographically resolved isomeric metabolites, features **F2**, **F4**, and **F7**, had the elemental composition $C_{16}H_{18}O_9$ and exhibited fragmentation patterns characteristic of mono-caffeoylquinic acids. Their probable regioisomeric structures showed MS/MS patterns consistent with the diagnostic fragmentation hierarchy established for caffeoylquinic acid regioisomers [49]. The MS/MS spectrum of feature **F7** was strongly dominated by the quinic acid ion at m/z 191, formed upon cleavage of the caffeoyl residue, whereas the other ions were absent or of very low abundance. Feature **F2** also generated m/z 191 as the base peak; however, an abundant product ion at m/z 179, corresponding to deprotonated caffeic acid, was additionally observed. In contrast, the MS/MS spectrum of feature **F4** was dominated by m/z 173, assigned to $[\text{Quinic acid} - \text{H} - \text{H}_2\text{O}]^-$, while the ions at m/z 191 and 179 each reached approximately 60% relative intensity. These fragmentation patterns are consistent with the established behavior of caffeoylquinic acid regioisomers: 3- and 5-*O*-caffeoylquinic acids predominantly yield m/z 191, with a substantially greater contribution of m/z 179 for 3-CQA, whereas 4-acyl substitution favors formation of the diagnostic dehydrated quinic acid ion at m/z 173 [49]. Accordingly, features **F7**, **F4**, and **F2** were putatively annotated as 5-*O*-caffeoylquinic acid (5-CQA), 4-*O*-caffeoylquinic acid (4-CQA), and 3-*O*-caffeoylquinic acid (3-CQA), respectively. The observed elution order of the putatively annotated mono-caffeoylquinic acid isomers differs from the sequence commonly reported for conventional reversed-phase C18 chromatography (3-CQA, 5-CQA, and 4-CQA). However, previous studies have demonstrated that the relative retention of 4-CQA and 5-CQA depends on stationary-phase selectivity, and that their elution order may be reversed under certain chromatographic conditions [50]. A related series of three metabolites features **F12**, **F14**, and **F16**, which showed $[\text{M} - \text{H}]^-$ ions and fragmentation patterns characteristic of dicaffeoylquinic acids. Their MS/MS spectra showed diagnostic differences consistent with the established fragmentation hierarchy for caffeoylquinic acid regioisomers [51]. Feature **F14** was characterized by predominant formation of the m/z 191 ion and only minor contribution from m/z 173, supporting its annotation as 3,5-di-*O*-caffeoylquinic acid (3,5-diCQA). In contrast, features **F12** and **F16** exhibited intense m/z 173 ions, indicating the presence of a 4-*O*-caffeoyl substituent. These two isomers were further distinguished by the dehydrated caffeoylquinic acid product at m/z 335, which was appreciable for feature **F12** but negligible for feature **F16**. The compounds were therefore annotated as 3,4-di-*O*-caffeoylquinic (3,4-diCQA) acid and 4,5-di-*O*-caffeoylquinic acid (4,5-diCQA), respectively.

Several additional hydroxycinnamate conjugates were associated with the same molecular family. Features **F3** and **F6** underwent a neutral loss of 162.05 Da to yield the caffeate ion at m/z 179, followed by its characteristic decarboxylation product at m/z 135, and were therefore annotated as isomeric caffeic acid hexosides. Feature **F5** showed loss of 162.05 Da to yield the ion at m/z 163.04, consistent with deprotonated *p*-coumaric acid; the abundant product at m/z 119.05 corresponded to its subsequent decarboxylation; it was consequently assigned as a hydroxycinnamic acid hexoside, putatively a *p*-coumaric acid hexoside. Finally, feature **F8** was annotated as caffeoylshikimic acid based on its $[\text{M} - \text{H}]^-$ ion at m/z 335 and the characteristic formation of the caffeate-derived ions at m/z 179, 161, and 135.

4. Discussion

Previous phytochemical studies of *P. dubium* have focused predominantly on alkaloids, particularly those occurring in cultured material or underground organs, and have reported

magnoflorine, jatrorrhizine, berberine, and related isoquinoline alkaloids [14,16,17]. The present untargeted analysis substantially broadens this phytochemical composition. In addition to a structurally diverse set of benzylisoquinoline-derived alkaloids, the metabolite profile contained an extensive family of triterpene saponins together with flavonoid glycosides and hydroxycinnamate-related metabolites. These findings indicate that the metabolite profile of *P. dubium* is considerably more diverse than suggested by earlier studies. The alkaloid-related profiles showed marked differences between the root and aerial-part extracts. Magnoflorine was the dominant annotated alkaloid-related feature in the roots, consistent with a previous LC-MS study of the underground parts of *P. dubium* in which magnoflorine was reported among the major constituents [14]. In contrast, the aerial-part profile was dominated by two jatrorrhizine/columbamine isomers. Jatrorrhizine has previously been isolated from cultured cells of *P. dubium* [16], whereas both jatrorrhizine and columbamine were subsequently detected by LC-MS in the underground parts of this species [14]. These alkaloids are also well-established constituents of protoberberine-producing Berberidaceae, including species of *Berberis* [12]. Notably, berberine, previously reported from *P. dubium*, and berberrubine, reported as a major constituent of the underground parts, were not detected among the annotated features under the present analytical conditions [14,17]. Differences in geographic origin, collection season, and developmental state may contribute to these discrepancies.

The annotated alkaloid-related features encompassed several branches of benzylisoquinoline-derived metabolism, including aporphines, monomeric and putative dimeric protoberberines, and benzyltetrahydroisoquinoline derivatives. Reticuline is a central intermediate in benzylisoquinoline alkaloid biosynthesis and is converted by berberine bridge enzyme to (*S*)-scoulerine, a precursor of tetrahydroprotoberberine and protoberberine alkaloids [7]. Its occurrence together with jatrorrhizine/columbamine-type metabolites and palmatine is therefore consistent with the established biosynthetic relationships among these alkaloid classes. The additional occurrence of oxygenated, glycosylated, and other modified protoberberine-related features indicates substantial diversification of this metabolite pool. Feature **A9** was particularly unusual because its MS/MS spectrum was consistent with a jatrorrhizine/columbamine-type core exhibiting a neutral loss corresponding to $C_{10}H_{12}O_4$. Rare phenylpropanoid-conjugated protoberberines provide a structural precedent: decumicorine A and epi-decumicorine A from *Corydalis decumbens* contain a jatrorrhizine core conjugated with a phenylpropanoid-derived moiety [52]. The $C_{10}H_{12}O_4$ composition inferred for **A9** contains two more hydrogen atoms than ferulic acid ($C_{10}H_{10}O_4$), suggesting a potentially related, more reduced motif. However, this remains only a structural analogy because neither the identity nor the attachment mode of the $C_{10}H_{12}O_4$ moiety in **A9** can be established from the present MS/MS data. The bisjatrorrhizine-type features **A12** and **A13** represent another unusual component of the alkaloid profile. Their elemental composition is identical to that reported for bisjatrorrhizine, a naturally occurring dimeric protoberberine originally isolated from *Jatrorrhiza palmata* [53]. Oxidative coupling provides a plausible biochemical precedent, as enzymatic formation of 4,4′-bisjatrorrhizine from jatrorrhizine has been demonstrated using a peroxidase from *Berberis stolonifera* cell cultures [54].

Taken together, the alkaloid-related profiles of the two analyzed plant parts differed not only in overall signal intensity but also in the relative contributions of distinct structural groups. The root profile was strongly dominated by magnoflorine and showed greater contributions from several oxygenated, glycosylated, and other modified alkaloid-related features, whereas the aerial-part profile was characterized by a larger relative contribution from jatrorrhizine/columbamine-type protoberberines and related compounds.

The glycoside profile of *P. dubium* showed substantial compositional diversity. The inferred aglycone compositions are not unique to a particular triterpenoid structure and

may correspond to different combinations of oxygen-containing functional groups. Several structurally characterized sapogenins with these elemental compositions have been reported in the literature, including compounds containing one or two carboxyl groups. These examples are discussed to illustrate the structural diversity associated with the proposed molecular formulas rather than to suggest that the same aglycones occur in *P. dubium*. In the present study, the predominance of $[M + HCOO]^-$ ions may favor structural models lacking readily ionizable free carboxyl groups, although this interpretation is not conclusive. Among the five inferred aglycone families, the $C_{30}H_{46}O_7$ was predominant and comprised 35 chromatographic components containing Pent–Hex–Hex (14 components), Pent–Hex–Pent (14 components), or Hex–Pent (7 components) carbohydrate moieties. Several structurally characterized pentacyclic sapogenins with the same elemental composition have been reported. These include zanhic acid [55], presenegenin [56], bartogenic acid [57], 20(*S*)-3β,19α,24-trihydroxyurs-12-ene-23,28-dioic acid [58], and corosin [59]. Although differing in carbon skeleton and substitution pattern, these compounds share a common degree of oxidation and are characterized by three hydroxyl groups and two carboxyl groups. Thus, the $C_{30}H_{46}O_7$ composition observed in the present dataset is compatible with a highly oxygenated dicarboxylic oleanane- or ursane-type sapogenin. Seventeen components were assigned to the $C_{30}H_{46}O_6$ aglycone family. This elemental composition is likewise represented by several structurally distinct pentacyclic sapogenins. Examples containing two carboxyl and two hydroxyl groups include medicagenic acid [60], 16α-hydroxygypsogenic acid [61], dianic acid [62], and myriaboric acid [63]. Alternatively, the same molecular formula can arise from sapogenins containing three hydroxyl groups, one carboxyl group, and an additional ketone function, as exemplified by bellisonic acid [64] and 11-oxo-caulophyllogenin. Notably, 11-oxo-caulophyllogenin-derived saponins have previously been characterized in *Caulophyllum robustum* by LC-QTOF MS, providing a chemotaxonomically relevant precedent for the occurrence of highly oxygenated oxo-substituted triterpene aglycones within the Berberidaceae. The highly similar product-ion patterns observed for the $C_{30}H_{46}O_6$- and $C_{30}H_{46}O_7$-containing saponins suggest that these aglycone families are structurally closely related. In particular, the $C_{30}H_{46}O_7$ sapogenin may represent an additionally oxygenated, possibly hydroxylated, analogue of the $C_{30}H_{46}O_6$ aglycone. Considering the observed ionization behavior and structural precedents among saponins from related Berberidaceae species, an oleanane-type model containing hydroxyl and carbonyl functionalities, but no free carboxyl groups, was proposed as one possible structural interpretation (Figure 3). An oxo functionality at C-11 was included as a plausible structural hypothesis based on the occurrence of 11-oxo-substituted sapogenins, including 11-oxo-caulophyllogenin derivatives, in the closely related Berberidaceae genus Caulophyllum [19]. However, localization of the oxidation at C-11 remains tentative and requires isolation and NMR characterization.

Four components were assigned to an aglycone composition of $C_{29}H_{44}O_7$. The loss of one carbon atom relative to the predominant C_{30}-aglycones is compatible with a nortriterpene sapogenin; however, its precise carbon skeleton and the position of carbon loss could not be established. Finally, a single component was associated with the $C_{30}H_{48}O_6$ aglycone family, indicating the presence of a minor, more highly hydrogenated C_{30}-sapogenin type within the glycoside profile.

Di- and trisaccharide moieties containing combinations of pentose and hexose residues are well documented among pentacyclic triterpene saponins, although the specific linear arrangement with a terminal pentose residue is less common. For example, saponins isolated from *Bongardia chrysogonum* (Berberidaceae) contain a linear β-D-Glc-(1 → 4)-β-D-Glc-(1 → 4)-α-L-Ara- chain [65], corresponding to the same overall Pent + 2Hex composition observed for the major group in the present study, although with the pentose directly

attached to the aglycone rather than occupying the non-reducing terminus. The carbohydrate moieties of triterpene saponins most frequently comprise arabinose and glucose residues, although xylose, galactose, and other monosaccharides may also be present. Glycosylation most commonly involves the C-3 hydroxyl group of the aglycone, while saponins possessing a C-28 carboxyl group may additionally or alternatively form a glycosyl ester at this position. Both 3-*O*-monodesmosidic and 3,28-bidesmosidic architectures are widely represented among oleanane-type saponins. Less common glycosylation patterns involving other hydroxylated positions have also been structurally characterized, including C-16, C-21, and C-22 [66]. The shorter Hex–Pent and Hex–Hex carbohydrate moieties are compositionally related to the corresponding Pent–Hex–Pent and Pent–Hex–Hex trisaccharides, respectively, through the absence of a terminal pentose residue. These compounds may therefore represent biosynthetic intermediates or products of enzymatic deglycosylation of the corresponding trisaccharides following removal of a terminal pentose unit.

The variable non-carbohydrate R_1 moiety represented another distinctive feature of the saponin family. The assigned R_1 compositions $C_6H_{10}O_4$–$C_{10}H_{18}O_4$ form a homologous series differing successively by CH_2 and are compositionally consistent with saturated aliphatic dicarboxylic acids among other possible oxygenated structural motifs. Dicarboxylic acid-containing structural motifs have previously been reported in triterpene saponins, including unusual dicarboxylic acid-substituted oleanane saponins from *Bassia indica* and sugar beet [67,68]. The recurrent C_5-derived acyl modification also has structural precedents among triterpene saponins. For example, 2-methylbutanoyl groups have been identified at aglycone hydroxy groups in saponins from *Camellia sinensis* and *Maesa japonica* [43,44], whereas isovaleryl groups occur on barringtogenol C derivatives from *Foetidia africana* [45].

Overall, the semi-quantitative data revealed marked differences in the relative LC–MS signals of saponin-related features between the two extracts of *P. dubium*. The summed saponin-related LC-MS signals were broadly comparable between the two organs, but primarily in the relative contribution of distinct sapogenin, oligosaccharide, and non-carbohydrate substituent families. Aerial tissues were strongly enriched in the more highly oxygenated $C_{30}H_{46}O_7$ sapogenin family and Pent–Hex–Pent-containing glycosides, whereas roots contained a substantially greater contribution of $C_{30}H_{46}O_6$-derived and shorter-chain saponins. In contrast, the recurrent C_5-derived acyl modification was abundant in both organs and therefore appears to represent a general structural characteristic of the major saponin pool rather than an organ-specific modification. The coordinated differences in aglycone formula, glycan composition, and R1 composition suggest that the contrasting profiles do not arise from changes in a single modification step. Rather, several late-stage processes, including aglycone oxidation, glycosylation, and addition of non-carbohydrate moieties, may contribute to the observed divergence between the two extracts.

To the best of our knowledge, triterpene saponins have not previously been reported from *P. dubium*. None of the major saponin features could be assigned unambiguously to previously characterized compounds on the basis of available spectral and literature data. The extensive structural diversity observed here therefore suggests that *P. dubium* may represent a rich source of previously uncharacterized triterpene glycosides. Isolation of the major components followed by NMR and complementary spectroscopic analyses will be required to establish their complete structures.

The strong aerial enrichment of flavonoid glycosides and hydroxycinnamate derivatives contrasted with the root enrichment observed for several alkaloid-related features. The summed LC-MS signal of the flavonoid molecular family was substantially higher in the aerial parts, and several kaempferol glycosides were detected exclusively or almost exclusively in these tissues. Hydroxycinnamate derivatives showed a similar, although less extreme, tendency, with all annotated mono- and dicaffeoylquinic acids displaying

substantially higher signals in the aerial parts. In contrast, the comparatively weak root profile was dominated by quinic acid and 4-*O*-caffeoylquinic acid.

An important limitation of the present study is the use of pooled plant material. Roots and aerial parts collected from ten individuals were combined into two composite samples, and individual plants were not analyzed separately. Consequently, the observed differences in LC-MS profiles describe the relative distribution of metabolite-related signals between the two pooled extracts but do not provide information on inter-individual variability or the statistical significance of organ-associated differences. Further studies involving independent biological replicates will be necessary to evaluate the reproducibility of these differences and establish whether they reflect consistent organ-dependent patterns of metabolite accumulation. It should also be acknowledged that the drying and extraction procedures may have affected the stability of certain metabolites. Therefore, some differences between the detected metabolite profiles and the native phytochemical composition of the plant material may be attributable to sample preparation.

The contrasting metabolite profiles of the roots and aerial parts may also have functional significance. The strong enrichment of flavonoid glycosides and hydroxycinnamate derivatives in the aerial tissues is consistent with the well-established roles of these metabolite classes in photoprotection, attenuation of UV radiation, and responses to oxidative and herbivore-associated stress in photosynthetically active organs [69,70]. In contrast, the pronounced accumulation of magnoflorine and several oxygenated, glycosylated, and conjugated alkaloid derivatives in the roots may reflect a greater contribution of benzylisoquinoline alkaloids to chemical defense or storage in belowground tissues. Such differences could arise from organ-specific regulation of biosynthesis, inter-organ transport, or differences in metabolite turnover.

5. Conclusions

Untargeted LC-HRMS/MS profiling combined with feature-based molecular networking provided a broad overview of the secondary metabolite composition of the roots and aerial parts of *P. dubium*. The analysis revealed marked differences between the root and aerial-part metabolite profiles and enabled putative annotation of structurally diverse isoquinoline alkaloids, triterpene saponins, flavonoid glycosides, and hydroxycinnamic acid derivatives. Particularly notable was the extensive family of triterpene saponins, comprising numerous combinations of highly oxygenated aglycones, oligosaccharide moieties, and non-carbohydrate substituents, many of which could not be matched to previously characterized compounds. The results therefore indicate that *P. dubium* contains a substantially greater chemical diversity than suggested by previous phytochemical studies and may represent a rich source of previously uncharacterized natural products. At the same time, the structural information obtainable from LC-MS/MS remains insufficient for unambiguous determination of carbon skeletons, substitution positions, monosaccharide identities, and stereochemistry. Isolation of the major and structurally distinctive metabolites followed by NMR and complementary spectroscopic analyses will therefore be essential to establish their complete structures and confirm whether they represent new natural products.

Supplementary Materials: The following supporting information can be downloaded at https://www.mdpi.com/article/10.3390/separations13110323/s1, Figure S1. Base-peak chromatograms of root and aerial-part extracts of *Plagiorhegma dubium* obtained by LC-MS/MS in negative- and positive-ion modes. (A) Roots, negative-ion mode; (B) aerial parts, negative-ion mode; (C) roots, positive-ion mode; (D) aerial parts, positive-ion mode; Figure S2. Feature-based molecular network of metabolites detected in the roots and aerial parts of *P. dubium* by positive-ion LC-MS/MS. Nodes represent individual features, whereas edges connect features with similar MS/MS fragmentation patterns. Pie-chart sectors indicate the relative contribution of root (blue) and aerial-part (green)

extracts to the corresponding feature signal, and node size is proportional to the summed LC-MS signal; Figure S3. Feature-based molecular network of metabolites detected in the roots and aerial parts of *P. dubium* by negative-ion LC-MS/MS. Nodes represent individual features, whereas edges connect features with similar MS/MS fragmentation patterns. Pie-chart sectors indicate the relative contribution of root (blue) and aerial-part (green) extracts to the corresponding feature signal, and node size is proportional to the summed LC-MS signal; Table S1. LC–MS/MS characteristics and relative abundances of putatively annotated alkaloids detected in the roots and aerial parts of *P. dubium* in positive-ion mode; Figure S4. Positive-ion MS/MS spectra of the putatively annotated alkaloid-related features detected in the roots and aerial parts of *P. dubium*. Feature IDs (A1–A7) correspond to those listed in Table S1; Figure S5. Positive-ion MS/MS spectra of the putatively annotated alkaloid-related features detected in the roots and aerial parts of *Plagiorhegma dubium*. Feature IDs (A8–A14) correspond to those listed in Table S1; Table S2. LC-HRMS/MS characteristics, putative compositional assignments, and peak-area distributions of triterpenoid saponin-related features in root and aerial-part extracts of *P. dubium*; Table S3. LC–MS/MS characteristics and relative signals of putatively annotated flavonoid, hydroxycinnamate, and related metabolites detected in the roots and aerial parts of *P. dubium* in negative-ion mode; Table S4. Parameters used for data preprocessing in MZmine.

Author Contributions: Conceptualization, R.S.P., E.V.N. and P.S.D.; methodology, R.S.P.; formal analysis, R.S.P.; investigation, R.S.P. and N.V.I.; resources, E.V.N. and R.V.D.; writing—original draft preparation, R.S.P., N.V.I.; writing—review and editing, E.V.N., R.V.D. and P.S.D.; supervision, P.S.D. All authors have read and agreed to the published version of the manuscript.

Funding: This research was funded by Russian Science Foundation (RSF), grant number 25-24-00397.

Data Availability Statement: The feature-based molecular networking results generated in this study are publicly available through the GNPS platform. The GNPS jobs for the positive- and negative-ion datasets can be accessed at https://gnps.ucsd.edu/ProteoSAFe/status.jsp?task=323d8eb2a14b4b04907b0eee55ddad24 (accessed on 1 September 2026) and https://gnps.ucsd.edu/ProteoSAFe/status.jsp?task=041f9892f911410087ae0efe713a6680 (accessed on 1 September 2026), respectively.

Acknowledgments: The study was carried out on the equipment of the Collective Facilities Center "The Far Eastern Center for Structural Molecular Research (NMR/MS) PIBOC FEB RAS".

Conflicts of Interest: The authors declare no conflicts of interest.

Abbreviations

The following abbreviations are used in this manuscript:

CID	Collision-induced dissociation
CQA	Caffeoylquinic acid
ESI	Electrospray ionization
FBMN	Feature-based molecular networking
GNPS	Global Natural Products Social Molecular Networking
Hex	Hexose residue
HPLC	High-performance liquid chromatography
HRMS/MS	High-resolution tandem mass spectrometry
LC	Liquid chromatography
MS	Mass spectrometry
MS/MS	Tandem mass spectrometry
NMR	Nuclear magnetic resonance
Pent	Pentose residue
QA	Quinic acid
QTOF	Quadrupole time-of-flight
Rt	Retention time
UHPLC	Ultra-high-performance liquid chromatography

References

1. Erb, M.; Kliebenstein, D.J. Plant Secondary Metabolites as Defenses, Regulators, and Primary Metabolites: The Blurred Functional Trichotomy. *Plant Physiol.* **2020**, *184*, 39–52. [CrossRef] [PubMed]
2. Latif, R.; Nawaz, T. Medicinal Plants and Human Health: A Comprehensive Review of Bioactive Compounds, Therapeutic Effects, and Applications. *Phytochem. Rev.* **2026**, *25*, 2299–2342. [CrossRef]
3. Butler, M.S.; La Clair, J.J. The Role of Natural Product Chemistry in Drug Discovery: Two Decades of Progress and Perspectives. *J. Nat. Prod.* **2026**, *89*, 3–28. [CrossRef] [PubMed]
4. Dixon, R.A.; Dickinson, A.J. A Century of Studying Plant Secondary Metabolism—from "What?" To "Where, How, and Why?". *Plant Physiol.* **2024**, *195*, 48–66. [CrossRef] [PubMed]
5. Plants of the World Online. Berberidaceae Juss. Available online: https://powo.science.kew.org/taxon/urn%3Alsid%3Aipni.org%3Anames%3A30000989-2 (accessed on 15 August 2026).
6. Potdar, D.; Hirwani, R.R.; Dhulap, S. Phyto-Chemical and Pharmacological Applications of *Berberis aristata*. *Fitoterapia* **2012**, *83*, 817–830. [CrossRef] [PubMed]
7. Jiang, W.; Zhang, W.; Jing, C.; Zhou, H.; Zhang, Z.-J.; Wang, R.; Liu, Y.-Q. Plant Protoberberine Alkaloids: Structural Diversity, Biosynthesis, Synthesis, Biological Activity, Structure-Activity Relationships and Clinical Applications of Berberine. *Phytochemistry* **2026**, *242*, 114690. [CrossRef] [PubMed]
8. Ma, H.; He, X.; Yang, Y.; Li, M.; Hao, D.; Jia, Z. The Genus Epimedium: An Ethnopharmacological and Phytochemical Review. *J. Ethnopharmacol.* **2011**, *134*, 519–541. [CrossRef] [PubMed]
9. Bastos, J.K.; Burandt, C.L.; Nanayakkara, N.P.D.; Bryant, L.; McChesney, J.D. Quantitation of Aryltetralin Lignans in Plant Parts and among Different Populations of *Podophyllum peltatum* by Reversed-Phase High-Performance Liquid Chromatography. *J. Nat. Prod.* **1996**, *59*, 406–408. [CrossRef]
10. Motyka, S.; Jafernik, K.; Ekiert, H.; Sharifi-Rad, J.; Calina, D.; Al-Omari, B.; Szopa, A.; Cho, W.C. Podophyllotoxin and Its Derivatives: Potential Anticancer Agents of Natural Origin in Cancer Chemotherapy. *Biomed. Pharmacother.* **2023**, *158*, 114145. [CrossRef] [PubMed]
11. Yu, X.; He, L.; Li, G.; Guo, Y.; Kuang, H.; Lv, S. *Caulophyllum robustum* Maxim in the Management of Rheumatoid Arthritis: A Comprehensive Review of Ethnopharmacology, Phytochemistry, Pharmacokinetics, and Pharmacological Mechanisms. *Front. Pharmacol.* **2026**, *17*, 1863086. [CrossRef] [PubMed]
12. Och, A.; Lemieszek, M.K.; Cieśla, M.; Jedrejek, D.; Kozłowska, A.; Pawelec, S.; Nowak, R. Berberis Vulgaris L. Root Extract as a Multi-Target Chemopreventive Agent against Colon Cancer Causing Apoptosis in Human Colon Adenocarcinoma Cell Lines. *Int. J. Mol. Sci.* **2024**, *25*, 4786. [CrossRef] [PubMed]
13. Xia, Y.-G.; Li, G.-Y.; Liang, J.; Yang, B.-Y.; Lü, S.-W.; Kuang, H.-X. Genus *Caulophyllum*: An Overview of Chemistry and Bioactivity. *Evid.-Based Complement. Altern. Med.* **2014**, *2014*, 684508. [CrossRef] [PubMed]
14. Sun, H.; Chen, M.; He, X.; Sun, Y.; Feng, J.; Guo, X.; Li, L.; Zhu, J.; Xia, G.; Zang, H. Phytochemical Analysis and in Vitro and in Vivo Antioxidant Properties of *Plagiorhegma dubia* Maxim as a Medicinal Crop for Diabetes Treatment. *Arab. J. Chem.* **2023**, *16*, 104788. [CrossRef]
15. Peng, Y. A Pharmacophylogenetic Study of the Berberidaceae (s.l.). *Acta Phytotaxon. Sin.* **2006**, *44*, 241. [CrossRef]
16. Arens, H.; Fischer, H.; Leyck, S.; Römer, A.; Ulbrich, B. Antiinflammatory Compounds from *Plagiorhegma dubium* Cell Culture. *Planta Med.* **1985**, *51*, 52–56. [CrossRef] [PubMed]
17. Jeong, B.R.; Sivanesan, I. Micropropagation, Berberine Content and Antitumor Activity of *Jeffersonia dubia* (Maxim.) Benth et Hook. *Plant Cell Tissue Organ Cult. (PCTOC)* **2016**, *124*, 453–458. [CrossRef]
18. Nova-Baza, D.; Olivares-Caro, L.; Bustamante, L.; Pérez, A.J.; Vergara, C.; Fuentealba, J.; Mardones, C. Metabolic Profile and Antioxidant Capacity of Five Berberis Leaves Species: A Comprehensive Study to Determine Their Potential as Natural Food or Ingredient. *Food Res. Int.* **2022**, *160*, 111642. [CrossRef] [PubMed]
19. Xia, Y.-G.; Li, G.-Y.; Liang, J.; Ortori, C.A.; Yang, B.-Y.; Kuang, H.-X.; Barrett, D.A. A Strategy for Characterization of Triterpene Saponins in *Caulophyllum robustum* Hairy Roots by Liquid Chromatography with Electrospray Ionization Quadrupole Time-of-Flight Mass Spectrometry. *J. Pharm. Biomed. Anal.* **2014**, *100*, 109–122. [CrossRef] [PubMed]
20. Alvarez-Rivera, G.; Ballesteros-Vivas, D.; Parada-Alfonso, F.; Ibañez, E.; Cifuentes, A. Recent Applications of High Resolution Mass Spectrometry for the Characterization of Plant Natural Products. *TrAC Trends Anal. Chem.* **2019**, *112*, 87–101. [CrossRef]
21. Sasse, M.; Rainer, M. Mass Spectrometric Methods for Non-Targeted Screening of Metabolites: A Future Perspective for the Identification of Unknown Compounds in Plant Extracts. *Separations* **2022**, *9*, 415. [CrossRef]
22. Nothias, L.-F.; Petras, D.; Schmid, R.; Dührkop, K.; Rainer, J.; Sarvepalli, A.; Protsyuk, I.; Ernst, M.; Tsugawa, H.; Fleischauer, M.; et al. Feature-Based Molecular Networking in the GNPS Analysis Environment. *Nat. Methods* **2020**, *17*, 905–908. [CrossRef] [PubMed]

23. Sumner, L.W.; Amberg, A.; Barrett, D.; Beale, M.H.; Beger, R.; Daykin, C.A.; Fan, T.W.-M.; Fiehn, O.; Goodacre, R.; Griffin, J.L.; et al. Proposed Minimum Reporting Standards for Chemical Analysis: Chemical Analysis Working Group (CAWG) Metabolomics Standards Initiative (MSI). *Metabolomics* **2007**, *3*, 211–221. [CrossRef] [PubMed]
24. Chambers, M.C.; Maclean, B.; Burke, R.; Amodei, D.; Ruderman, D.L.; Neumann, S.; Gatto, L.; Fischer, B.; Pratt, B.; Egertson, J.; et al. A Cross-Platform Toolkit for Mass Spectrometry and Proteomics. *Nat. Biotechnol.* **2012**, *30*, 918–920. [CrossRef] [PubMed]
25. Pluskal, T.; Castillo, S.; Villar-Briones, A.; Orešič, M. MZmine 2: Modular Framework for Processing, Visualizing, and Analyzing Mass Spectrometry-Based Molecular Profile Data. *BMC Bioinform.* **2010**, *11*, 395. [CrossRef] [PubMed]
26. Wang, M.; Carver, J.J.; Phelan, V.V.; Sanchez, L.M.; Garg, N.; Peng, Y.; Nguyen, D.D.; Watrous, J.; Kapono, C.A.; Luzzatto-Knaan, T.; et al. Sharing and Community Curation of Mass Spectrometry Data with Global Natural Products Social Molecular Networking. *Nat. Biotechnol.* **2016**, *34*, 828–837. [CrossRef] [PubMed]
27. Shannon, P.; Markiel, A.; Ozier, O.; Baliga, N.S.; Wang, J.T.; Ramage, D.; Amin, N.; Schwikowski, B.; Ideker, T. Cytoscape: A Software Environment for Integrated Models of Biomolecular Interaction Networks. *Genome Res.* **2003**, *13*, 2498–2504. [CrossRef] [PubMed]
28. Stévigny, C.; Jiwan, J.-L.H.; Rozenberg, R.; De Hoffmann, E.; Quetin-Leclercq, J. Key Fragmentation Patterns of Aporphine Alkaloids by Electrospray Ionization with Multistage Mass Spectrometry. *Rapid Commun. Mass Spectrom.* **2004**, *18*, 523–528. [CrossRef] [PubMed]
29. Singh, A.; Bajpai, V.; Kumar, S.; Singh Rawat, A.K.; Kumar, B. Analysis of Isoquinoline Alkaloids from *Mahonia leschenaultia* and *Mahonia napaulensis* Roots Using UHPLC-Orbitrap-MSn and UHPLC-QqQLIT-MS/MS. *J. Pharm. Anal.* **2017**, *7*, 77–86. [CrossRef] [PubMed]
30. Qing, Z.; Xu, Y.; Yu, L.; Liu, J.; Huang, X.; Tang, Z.; Cheng, P.; Zeng, J. Investigation of Fragmentation Behaviours of Isoquinoline Alkaloids by Mass Spectrometry Combined with Computational Chemistry. *Sci. Rep.* **2020**, *10*, 733. [CrossRef] [PubMed]
31. Fan, M.; Tian, Y.; Chen, G.; Sarker, S.D.; Nahar, L.; Wu, J.; Li, N.; Guo, M. Enrichment and Analysis of Quaternary Alkaloids from *Zanthoxylum simulans* Using Weak Cation Exchange Solid-Phase Extraction Coupled with LC–MS. *Phytochem. Anal.* **2019**, *30*, 727–734. [CrossRef] [PubMed]
32. Zhang, Y.; Shi, Q.; Shi, P.; Zhang, W.; Cheng, Y. Characterization of Isoquinoline Alkaloids, Diterpenoids and Steroids in the Chinese Herb Jin-Guo-Lan (*Tinospora sagittata* and *Tinospora capillipes*) by High-performance Liquid Chromatography/Electrospray Ionization with Multistage Mass Spectrometry. *Rapid Commun. Mass Spectrom.* **2006**, *20*, 2328–2342. [CrossRef] [PubMed]
33. Tian, P.; Zhang, X.; Wang, H.; Li, P.; Liu, Y.; Li, S. Rapid Analysis of Components in Coptis Chinensis Franch by Ultra-Performance Liquid Chromatography with Quadrupole Time-of-Flight Mass Spectrometry. *Pharmacogn. Mag.* **2017**, *13*, 175–179. [PubMed]
34. Zhu, G.; Feng, F. Non-Targeted Metabolite Profiling and Specific Targeted Discrimination Strategy for Quality Evaluation of Cortex Phellodendri from Different Varieties. *RSC Adv.* **2018**, *8*, 22086–22094. [CrossRef] [PubMed]
35. Tian, Y.; Zhang, C.; Guo, M. Comparative Study on Alkaloids and Their Anti-Proliferative Activities from Three Zanthoxylum Species. *BMC Complement. Altern. Med.* **2017**, *17*, 460. [CrossRef] [PubMed]
36. E, S.; Shang, Z.-C.; Qin, S.; Li, K.; Liu, Y.; Wu, J.-L.; Yan, F.; Cai, W. A Systematic Method for the Identification of Aporphine Alkaloid Constituents in *Sabia schumanniana* Diels Using UHPLC-Q-Exactive Orbitrap/Mass Spectrometry. *Molecules* **2022**, *27*, 7643. [CrossRef] [PubMed]
37. Savarino, P.; Demeyer, M.; Decroo, C.; Colson, E.; Gerbaux, P. Mass Spectrometry Analysis of Saponins. *Mass Spectrom. Rev.* **2023**, *42*, 954–983. [CrossRef] [PubMed]
38. Ng, K.-M.; Che, C.-M.; Wo, S.-K.; Tam, P.K.-H.; Lau, A.S.-Y. Analytical Application of Acetate Anion in Negative Electrospray Ionization Mass Spectrometry for the Analysis of Triterpenoid Saponins–Ginsenosides. *Rapid Commun. Mass Spectrom.* **2006**, *20*, 1545–1550. [CrossRef] [PubMed]
39. Mad, T.; Sterk, H.; Mittelbach, M.; Rechberger, G.N. Tandem Mass Spectrometric Analysis of a Complex Triterpene Saponin Mixture of *Chenopodium quinoa*. *J. Am. Soc. Mass Spectrom.* **2006**, *17*, 795–806. [CrossRef] [PubMed]
40. Domon, B.; Costello, C.E. A Systematic Nomenclature for Carbohydrate Fragmentations in FAB-MS/MS Spectra of Glycoconjugates. *Glycoconj. J.* **1988**, *5*, 397–409. [CrossRef]
41. Feng, M.; Zhu, Z.; Zuo, L.; Chen, L.; Yuan, Q.; Shan, G.; Luo, S.-Z. A Strategy for Rapid Structural Characterization of Saponins and Flavonoids from the Testa of *Camellia oleifera* Abel Seeds by Ultra-High-Pressure Liquid Chromatography Combined with Electrospray Ionization Linear Ion Trap-Orbitrap Mass Spectrometry. *Anal. Methods* **2015**, *7*, 5942–5953. [CrossRef]
42. Strigina, L.I.; Chetyrina, N.S.; Isakov, V.V.; Dzizenko, A.K.; Elyakov, G.B. Caulophyllogenin: A Novel Triterpenoid from Roots of *Caulophyllum robustum*. *Phytochemistry* **1974**, *13*, 479–480. [CrossRef]
43. Lu, Y.; Umeda, T.; Yagi, A.; Sakata, K.; Chaudhuri, T.; Ganguly, D.K.; Sarma, S. Triterpenoid Saponins from the Roots of Tea Plant (*Camellia sinensis* Var. Assamica). *Phytochemistry* **2000**, *53*, 941–946. [CrossRef] [PubMed]

44. Koike, K.; Kudo, M.; Jia, Z.; Nikaido, T.; Ide, Y.; Sakura, T. New Triterpenoid Saponins from *Maesa japonica*. *J. Nat. Prod.* **1999**, *62*, 228–232. [CrossRef] [PubMed]
45. Crublet, M.-L.; Pouny, I.; Delaude, C.; Lavaud, C. Acylated Triterpenoid Saponins from the Stem Bark of *Foetidia africana*. *J. Nat. Prod.* **2002**, *65*, 1560–1567. [CrossRef] [PubMed]
46. Jiang, C.; Gates, P.J. Systematic Characterisation of the Fragmentation of Flavonoids Using High-Resolution Accurate Mass Electrospray Tandem Mass Spectrometry. *Molecules* **2024**, *29*, 5246. [CrossRef] [PubMed]
47. Cuyckens, F.; Claeys, M. Determination of the Glycosylation Site in Flavonoid Mono-*O*-Glycosides by Collision-Induced Dissociation of Electrospray-Generated Deprotonated and Sodiated Molecules. *J. Mass Spectrom.* **2005**, *40*, 364–372. [CrossRef] [PubMed]
48. Hvattum, E.; Ekeberg, D. Study of the Collision-Induced Radical Cleavage of Flavonoid Glycosides Using Negative Electrospray Ionization Tandem Quadrupole Mass Spectrometry. *J. Mass Spectrom.* **2003**, *38*, 43–49. [CrossRef] [PubMed]
49. Clifford, M.N.; Johnston, K.L.; Knight, S.; Kuhnert, N. Hierarchical Scheme for LC-MS Identification of Chlorogenic Acids. *J. Agric. Food Chem.* **2003**, *51*, 2900–2911. [CrossRef] [PubMed]
50. Deineka, L.A.; Deineka, V.I.; Blinova, I.P.; Oleinits, E.Y. Selectivity of the Separation of Isomeric Chlorogenic Acids under the Conditions of Reversed-Phase HPLC. *J. Anal. Chem.* **2019**, *74*, 778–783. [CrossRef]
51. Clifford, M.N.; Knight, S.; Kuhnert, N. Discriminating between the Six Isomers of Dicaffeoylquinic Acid by LC-MS^n. *J. Agric. Food Chem.* **2005**, *53*, 3821–3832. [CrossRef] [PubMed]
52. Lu, J.-G.; Wang, Y.; Yang, M.-R.; Wang, C.-Y.; Meng, J.; Liu, J.; Yang, Z.; Wu, K.; Bai, L.-P.; Zhu, G.-Y.; et al. Structures, Biomimetic Synthesis, and Anti-SARS-CoV-2 Activity of Two Pairs of Enantiomeric Phenylpropanoid-Conjugated Protoberberine Alkaloids from the Rhizomes of *Corydalis decumbens*. *Arch. Pharmacal Res.* **2022**, *45*, 631–643. [CrossRef] [PubMed]
53. Carvalhas, L. Bisjatrorrhizine, a New Dimeric Protoberberine Alkaloid from *Jatrorrhiza palmata* [Lam.] Miers. *J. Chem. Soc. Perkin 1* **1972**, *3*, 327–330. [CrossRef] [PubMed]
54. Hüttel, W.; Müller, M. Regio- and Stereoselective Intermolecular Phenol Coupling Enzymes in Secondary Metabolite Biosynthesis. *Nat. Prod. Rep.* **2021**, *38*, 1011–1043. [CrossRef] [PubMed]
55. Tava, A.; Biazzi, E.; Mella, M.; Quadrelli, P.; Avato, P. Artefact Formation during Acid Hydrolysis of Saponins from *Medicago* spp. *Phytochemistry* **2017**, *138*, 116–127. [CrossRef] [PubMed]
56. Mitaine-Offer, A.-C.; Miyamoto, T.; Khan, I.A.; Delaude, C.; Lacaille-Dubois, M.-A. Three New Triterpene Saponins from Two Species of *Carpolobia*. *J. Nat. Prod.* **2002**, *65*, 553–557. [CrossRef] [PubMed]
57. Rao, G.S.R.S.; Prasanna, S.; Kumar, V.P.S.; Mallavarapu, G.R. Bartogenic Acid, a New Triterpene Acid from *Barringtonia speciosa*. *Phytochemistry* **1981**, *20*, 333–334. [CrossRef]
58. Pires, V.S.; Gosmann, G.; Guillaume, D.; Schenkel, E.P. Triterpenes and Saponins from *Ilex psammophila*. *Nat. Prod. Lett.* **2002**, *16*, 401–406. [CrossRef] [PubMed]
59. Manzoor-i-Khuda, M.; Habermehl, G. Chemical Constituents of *Corchorus capsujaris* and *C. olitorius* (Jute Plant), III. Structure of Corosin. *Z. Naturforsch. C* **1974**, *29*, 209–221. [CrossRef]
60. Bialy, Z.; Jurzysta, M.; Mella, M.; Tava, A. Triterpene Saponins from the Roots of *Medicago hybrida*. *J. Agric. Food Chem.* **2006**, *54*, 2520–2526. [CrossRef] [PubMed]
61. Koike, K.; Jia, Z.; Nikaido, T. New Triterpenoid Saponins and Sapogenins from *Saponaria officinalis*. *J. Nat. Prod.* **1999**, *62*, 1655–1659. [CrossRef] [PubMed]
62. Park, S.-Y.; Yook, C.-S.; Nohara, T. New Oleanene Glycosides from the Leaves of *Acanthopanax japonicus*. *Chem. Pharm. Bull.* **2005**, *53*, 1147–1151. [CrossRef] [PubMed]
63. Ngounou, F.N.; Lontsi, D.; Sondengam, B.L. A Pentacyclic Triterpene Diacid from *Myrianthus arboreus*. *Phytochemistry* **1988**, *27*, 2287–2289. [CrossRef]
64. Schöpke, T.; Thiele, H.; Hiller, K.; Wray, V.; Nimtz, M. Triterpenoid Saponins from *Bellis bernardii*. *J. Nat. Prod.* **1996**, *59*, 939–943. [CrossRef] [PubMed]
65. Atta-ur-Rahman; Shahwar, D.; Choudhary, M.I.; Sener, B.; Toker, G.; Baser, K.H.C. Triterpenoid Saponins from *Bongardia chrysogonum*. *J. Nat. Prod.* **2000**, *63*, 251–253. [CrossRef] [PubMed]
66. Vincken, J.-P.; Heng, L.; De Groot, A.; Gruppen, H. Saponins, Classification and Occurrence in the Plant Kingdom. *Phytochemistry* **2007**, *68*, 275–297. [CrossRef] [PubMed]
67. Othman, A.; Amen, Y.; Shimizu, K. A Novel Acylated Flavonol Tetraglycoside and Rare Oleanane Saponins with a Unique Acetal-Linked Dicarboxylic Acid Substituent from the Xero-Halophyte *Bassia indica*. *Fitoterapia* **2021**, *152*, 104907. [CrossRef] [PubMed]
68. Edelmann, M.; Dawid, C.; Hochreiter, K.; Ralla, T.; Stark, T.D.; Salminen, H.; Weiss, J.; Hofmann, T. Molecularization of Foam-Active Saponins from Sugar Beet Side Streams (*Beta vulgaris* ssp. *Vulgaris* Var. *Altissima*). *J. Agric. Food Chem.* **2020**, *68*, 10962–10974. [CrossRef] [PubMed]

69. Treutter, D. Significance of Flavonoids in Plant Resistance and Enhancement of Their Biosynthesis. *Plant Biol.* **2005**, *7*, 581–591. [CrossRef] [PubMed]
70. Ferreyra, M.L.F.; Serra, P.; Casati, P. Recent Advances on the Roles of Flavonoids as Plant Protective Molecules after UV and High Light Exposure. *Physiol. Plant.* **2021**, *173*, 736–749. [CrossRef] [PubMed]

Disclaimer/Publisher's Note: The statements, opinions and data contained in all publications are solely those of the individual author(s) and contributor(s) and not of MDPI and/or the editor(s). MDPI and/or the editor(s) disclaim responsibility for any injury to people or property resulting from any ideas, methods, instructions or products referred to in the content.